

EVIDENCE FOR A SUBSEAFLOOR REPLACEMENT ORIGIN OF THE CRETACEOUS  
PALMA VOLCANOGENIC MASSIVE SULFIDE DEPOSIT, CENTRAL PERU

by  
Jeffrey McKeon

Copyright by Jeffrey McKeon 2019  
All Rights Reserved

A thesis submitted to the Faculty and Board of Trustees of the Colorado School of Mines  
in partial fulfillment of the requirements for the degree of Master of Science (Geology).

Golden, Colorado

Date \_\_\_\_\_

Signed: \_\_\_\_\_

Jeffrey McKeon

Signed: \_\_\_\_\_

Dr. Thomas Monecke

Thesis Advisor

Golden, Colorado

Date \_\_\_\_\_

Signed: \_\_\_\_\_

Dr. M. Stephen Enders

Professor and Head

Department of Geology and Geological Engineering

## ABSTRACT

The Palma volcanogenic massive sulfide deposit is one of the most recent significant base metal discoveries in central Peru. Base-metal mineralization can be followed over a strike length of over 2.5 km, with the currently best defined ore zone having an inferred resource of 5.59 million metric tons grading 7.43 wt % Zn, 1.50 wt % Pb, and 44.1 g/t Ag. The massive sulfides at Palma are hosted by a Cretaceous succession of hemipelagic mudstone that was intruded by basaltic dikes and sills. Contacts between the mafic intrusions and the enclosing carbonaceous mudstone are frequently marked by the occurrence of peperite suggesting that the emplacement of the high-level intrusions took place into the wet and unconsolidated sediments, broadly overlapping with the hydrothermal activity at Palma. Massive sulfide formation occurred ~50 m below the paleoseafloor through subseafloor infiltration and replacement of the mudstone host. Textural evidence suggests that the subseafloor replacement processes involved an early stage of carbonate alteration of the mudstone followed by sulfide replacement at increasingly higher temperatures. The carbonate alteration commonly occurs as bands of carbonate infiltration of the carbonaceous mudstone or as wispy, grey bands that contain mudstone clasts of various sizes that form a jigsaw in the carbonate matrix or have been rotated and abraded. The massive sulfides at Palma show many textural similarities to the carbonate-altered mudstone suggesting wholesale replacement of the carbonate by sulfides. Carbonate alteration associated with the concordant massive sulfides lenses overprinted the carbonaceous mudstone and mafic intrusions in the stratigraphic footwall, but decreases rapidly in intensity in the stratigraphic hangingwall of the ore bodies. The location of the paleoseafloor is marked by a ~20-m-thick package of mudstone that has experienced low-temperature hydrothermal clay alteration and silicification. Recent deep drilling into the stratigraphic footwall established the existence of a stringer zone containing abundant chalcopyrite, which are interpreted to represent a structurally controlled hydrothermal upflow zone. Following terrane accretion, the submarine mafic-siliciclastic rocks have been folded, with the Palma deposit today occurring on the eastern limb of an open, drag-folded anticline. The massive sulfides and their host rocks have been overprinted by contact metamorphism related to the emplacement of the Coastal batholith.

## TABLE OF CONTENTS

|   |     |
|---|-----|
| ABSTRACT .....  | iii |
| LIST OF FIGURES .....   | v   |
| ACKNOWLEDGEMENTS .....  | vi  |
| CHAPTER 1. EVIDENCE FOR A SUBSEAFLOOR REPLACEMENT ORIGIN OF<br>THE UPPER CRETACEOUS PALMA VOLCANOGENIC MASSIVE<br>SULFIDE DEPOSIT, CENTRAL PERU ..... | 1   |
| 1.1. Introduction .....   | 1   |
| 1.2. Regional Setting .....   | 2   |
| 1.3. Deposit Stratigraphy .....   | 5   |
| 1.4. Ore Zones .....  | 10  |
| 1.5. Gangue and Ore Textures .....  | 17  |
| 1.5.1. Carbonate textures .....   | 17  |
| 1.5.2. Silicified textures .....  | 19  |
| 1.5.3. Sulfide textures .....   | 24  |
| 1.6. Contact metamorphic overprint .....  | 25  |
| 1.7. Discussion .....   | 30  |
| 1.7.1. Depositional environment .....   | 30  |
| 1.7.2. Nature of the host rock succession .....   | 30  |
| 1.7.3. Relative timing of hydrothermal activity .....   | 33  |
| 1.7.4. Mechanisms of sulfide precipitation .....  | 34  |
| 1.7.5. Constraints on depth of seafloor replacement .....   | 35  |
| 1.7.6. Comparison to other deposits hosted by mudstone-dominated successions .....  | 36  |
| 1.8. Conclusions .....  | 38  |
| 1.9. References .....   | 41  |
| APPENDIX A SAMPLE TABLE .....   | 46  |

## LIST OF FIGURES

|  |    |
|--|----|
| Figure 1.1. Morphostructural units of the Peruvian Andes .....   | 7  |
| Figure 1.2. Geological map of the region southwest of Lima showing the outcrop area of Cretaceous submarine volcanic and sedimentary rocks and the location of the Palma deposit ..... | 8  |
| Figure 1.3. Geological map of the Palma deposit area showing the distribution of the different members of the Quilmaná Formation .....   | 12 |
| Figure 1.4. Graphical log of drill core 15057 that intersected the entire host rock stratigraphy of the Palma deposit.....   | 13 |
| Figure 1.5. Graphical logs of drill holes intersecting parts of the host rock stratigraphy of the Palma deposit .....  | 14 |
| Figure 1.6. Photographs of representative drill core from the host rock succession of the Palma deposit.....   | 15 |
| Figure 1.7. Cross-section of through the Palma deposit constructed using the advanced 3D modeling software Leapfrog .....  | 16 |
| Figure 1.8. Core photos of carbonate-altered mudstone. ....  | 21 |
| Figure 1.9. Microphotographs of carbonate-altered mudstone, carbonate-sulfide-altered mudstone, and sulfide-altered mudstone.....  | 23 |
| Figure 1.10. Core photos of sulfide textures.....  | 27 |
| Figure 1.11. Backscattered electron images of sulfide textural relationships.....  | 28 |
| Figure 1.12. Backscattered electron images of minerals formed as a result of the metamorphic overprint.....  | 31 |

## ACKNOWLEDGEMENTS

I'd like to express my extreme gratitude to my advisor, Dr. Thomas Monecke, for finding my project, providing support in field, and sharing his wealth of knowledge as a continued resource for the past two years. Without him, none of this would have been possible. I also thank my thesis advisory committee for guidance provided throughout the project. Many thanks to Dr. Richard Palin for providing a clear and refreshing take on the metamorphic petrology aspect of this project. I am indebted to Dr. Zhaoshan Chang for serving on my committee and providing his expert insight and feedback on an earlier version of this thesis.

I thank Volcan Compañía Minera for permission to study Palma and to publish the results of the work. The field work in Peru would not have been possible without the help of Marcelo Lavado and Cesar Emilio Farfan Bernales. They set-up the project and provided support in Peru. Both made sure that everything worked seamless during the field work. I also thank the geologists of Volcan Compañía Minera who helped me on site and discussed the regional and local geology with me in the field. Luis Fontboté is thanked for sharing his insights into the geology of the Peruvian VMS deposits. I am indebted to Dr. Katharina Pfaff for analytical help and training me in the use of the field emission electron microscope.

I thank my parents for the continued support during this mentally strenuous time. I would like to offer my gratitude to Hannah Cayes, for keeping me company during the entire writing process. I would have missed many deadlines if it weren't for her. I would also like to thank Isaac Simon, for his tireless support with the FE-SEM

CHAPTER 1  
EVIDENCE FOR A SUBSEAFLOOR REPLACEMENT ORIGIN OF THE UPPER  
CRETACEOUS PALMA VOLCANOGENIC MASSIVE SULFIDE DEPOSIT,  
CENTRAL PERU

A paper to be submitted to *Economic Geology*

Jeffrey McKeon<sup>1,2</sup>, Thomas Monecke<sup>1,3</sup>

This chapter discusses the results of a field-based study on the genesis of the Palma deposit in Peru. It has been prepared for submission to the journal *Economic Geology*.

### **1.1. Introduction**

The Palma volcanogenic massive sulfide (VMS) deposit is one of the most recent significant greenfields base metal discoveries in central Peru. Ongoing exploration at Palma has established that base metal mineralization can be followed over a strike length of over 2.5 km (Volcan Compañía Minera Annual Report 2016), with the currently best defined ore zone having an inferred resource of 5.590 million metric tonnes grading 7.43 wt % Zn, 1.50 wt % Pb, and 44.1 g/t Ag (Volcan Compañía Minera Reserves and Resources 2017). The Palma deposit is hosted by an Early Cretaceous succession of hemipelagic mudstone intruded by basaltic dikes and sills. Textural evidence suggests that the massive sulfides formed through subseafloor infiltration and replacement of the unconsolidated mudstone host.

Over the past decades, a number of studies have shown that subseafloor infiltration and replacement processes are key in making large VMS deposits as a higher proportion of metals can be contained in the subseafloor environment when compared to seafloor sulfide precipitation, which involves substantial metal loss into the ocean through black smoker activity (Gibson and Kerr, 1993; Doyle and Allen, 2003; Franklin et al., 2005; Piercey, 2015). The

---

<sup>1</sup>Graduate student and Associate Professor, respectively, Department of Geology and Geological Engineering, Colorado School of Mines

<sup>2</sup>Primary researcher and author

<sup>3</sup>Co-author

volcanic facies architecture of the host succession and the host rock permeability within tens of meters below the seafloor control whether sulfide deposits are formed at or immediately below the seafloor (Gibson et al., 1999; Monecke et al., 2017). Most well-documented examples of subseafloor deposits are hosted in highly permeable and glassy host rocks, including the products of mafic fire-fountain eruptions (Gibson et al., 1993; Gibson and Gamble, 2000), pumice-rich mass-flow deposits (Morton et al., 1991; Allen, 1994; Montelius et al., 2007), and coarse-grained volcanoclastic deposits associated with lavas and shallow intrusions such as cryptodomes (Galley et al., 1995; Doyle and Huston, 1999; Hannington et al., 1999; Monecke et al., 2008).

This contribution reports on the findings of a field-based study at the Palma VMS deposit aiming to constrain how subseafloor infiltration and replacement processes occur in fine-grained hemipelagic sediments. The study comprises a reconstruction of the volcanic facies architecture of the deposit and a detailed textural study of the variably altered and replaced mudstone host. Microanalytical work including optical microscopy and scanning electron microscopy was conducted to study the alteration of the host and the sulfide mineralogy. A TESCAN MIRA3 LMH Schottky field emission-scanning electron microscope (FE-SEM) equipped with a single-crystal YAG BSE detector and a Bruker XFlash 6/30 silicon drift detector was used for analysis. BSE imaging and EDS analyses were performed at a 15 keV or 20 keV acceleration voltage at a working distance of 10 mm and a beam intensity of 11. Emphasis was also placed on the mineralogical and textural reequilibration caused by contact metamorphism associated with the nearby Coastal batholith. The results of the study at Palma show that subseafloor replacement of the unconsolidated mudstone host involved early stage carbonate alteration followed by sulfide replacement at increasingly higher temperatures. The replacement processes occurred only tens of meters below the seafloor.

## **1.2. Regional Setting**

The host rocks of the Palma VMS deposit form part of a major belt of Cretaceous submarine volcanic and sedimentary rocks cropping out for a distance of ~1,200 km along the Pacific coast and Western Cordillera of Peru from Piura in northern Peru to Pisco in the south (Fig. 1.1). Traditionally, this belt of submarine volcanic and sedimentary rocks has been assigned to as the

Casma Group (Myers, 1974, 1980; Cobbing et al., 1981; Atherton et al., 1983; Vidal, 1987; Steinmüller et al., 2000). However, the geology of this belt of submarine volcanic and sedimentary rocks is comparably poorly constrained as previous mapping is largely restricted to areas hosting known VMS deposits and occurrences.

In the Lacones region of northern Peru, the Casma Group forms a package of bimodal volcanic and volcanoclastic rocks that are exposed over a strike length of ~135 km (Winter et al., 2010). Two main phases of volcanism have been recognized. Middle to late Albian volcanism (~105-100 Ma) resulted in the deposition of a ~2.5-km-thick mafic-dominated volcanic succession comprising primarily massive and pillowed lava flows and associated breccias deposits. Felsic volcanic rocks represent ~10 percent or less of the total volume of volcanic rocks. The Tambogrande deposit comprising several distinct massive sulfide lenses is closely associated with a ~2 km large rhyolite-dacite volcanic center that has a stratigraphic thickness of at least 300 m (Tegart et al., 2000; Winter, 2008; Winter et al., 2004, 2010). The largest orebody at Tambogrande (lens TG1) comprises 108.7 million tons grading 1.6 wt % Cu, 1.0 wt % Zn, 0.5 g/t Au, and 22 g/t Ag, with an additional 16.7 million tons of oxide ore grading 3.5 g/t Au and 64 g/t Ag. The second largest massive sulfide lens at Tambogrande (lens TG3) consists of 82 million tons grading 1.0 wt % Cu, 1.4 wt % Zn, 0.8 g/t Au, and 25 g/t Ag. The resource of an additional large (~100 million tons) massive sulfide orebody (lens B5) is undefined (Winter, 2008; Winter et al., 2004, 2010). A rhyolitic volcanoclastic deposit in the immediate hangingwall of the massive sulfides yielded a U-Pb zircon age of  $104.8 \pm 1.3$  Ma, constraining the minimum age of mineralization (Winter, 2008; Winter et al., 2010). The second phase of volcanism of the Casma Group occurred in the late Albian to Turonian (~99-91 Ma). Stratigraphically lowest is a ~2-km-thick mafic volcanoclastic-dominated succession that is overlain by a ~3.5-km-thick package of bimodal volcanic rocks. Mafic volcanic rocks primarily comprise massive lavas and associated autoclastic deposits. Quartz- and feldspar-phyric lavas and domes are common. Stratified volcanoclastic rocks make up a significant proportion of the bimodal volcanic package. Stratigraphically highest are thick volcanoclastic units that are intercalated with siliciclastic and notably calcareous rocks, including limestone, calcareous sandstone, siltstone, and graywacke (Tegart et al., 2000; Winter, 2008; Winter et al., 2010).

In the Huarmey region of central Peru, the Casma Group largely consists of massive flows and pillowed flows of mafic composition, thick autobreccia deposits, fine-grained volcanoclastic rocks composed of pumiceous and vitric material, and subordinate sedimentary deposits including chert, limestone, and siltstone. Minor rhyolitic flows have been recognized (Myers, 1980; Atheron and Webb, 1989). The Maria Teresa deposit represents the only VMS deposit known in the Huarmey region. The deposit has been intermittently mined for barite and base metals since 1973. The deposit includes ~ 1 million tons of ore grading 4 wt. % Zn, 2.2 wt. % Pb, 0.3 wt% Cu, and 100 g/t Ag (Steinmüller et al., 2000) that are hosted in fine-grained felsic volcanoclastic rocks (Vidal, 1987). The felsic deposits are overlain by basaltic lavas and associated autobreccia deposits (Vidal, 1987; Steinmüller et al., 2000).

In the Cañete region of central Peru, the Casma Group is host to the world-class Cerro Lindo VMS deposit. Mining at Cerro Lindo commenced in 2007. With past production of 39.9 Mt, and a current resource estimate of 87.4 Mt, the deposit totals 127.3 Mt of ore grading 2.6 wt. % Zn, 0.30 wt. % Pb, 0.79 wt. % Cu, and 25.5 g/t Ag (Dols and Monecke, 2018) The deposit consists of eight NW-SE-trending ore lenses formed within a felsic volcanic succession dominated by coherent rhyolite and associated breccias. Uranium-Pb zircon geochronology conducted on two rhyolite samples suggests that the felsic host rocks of Cerro Lindo formed between  $106.9 \pm 1.2$  Ma and  $105.7 \pm 1.0$  Ma (Milpo, unpublished technical report 2016), which is similar to the age of the volcanic succession hosting Tambogrande. Cerro Lindo and its host rocks form a roof pendant within the younger Coastal batholith and have experienced contact metamorphism.

In contrast to Tambogrande and Cerro Lindo hosted in late Albian to Turonian volcanic rocks of the Casma Group, several other VMS deposits in central Peru appear to be distinctly younger and are hosted in volcanic successions of Maastrichtian to Danian age. Traditionally the submarine volcanic host rocks of these deposits have also been assigned to the Casma Group. However, due to the substantial age difference, this assignment is likely not appropriate and stratigraphic revision may be needed as more age dating and mapping becomes available (Polliand et al., 2005; Romero, 2007).

The Perubar deposit in central Peru was mined between 1978 and 1999 (Table 1). The deposit comprised 5.6 million tons of ore grading 9.9 wt. % Zn and 1.4 wt. % Pb (Polliand and Fontboté, 2000). The footwall to the massive sulfides at this deposit is composed of a >600-m-thick succession of mudstone, siltstone, and sandstone that were extensively intruded by basalt sills. The siliciclastic sedimentary rocks are overlain by a ~150-m-thick bimodal volcanic succession of andesitic and rhyodacitic lavas and volcanoclastic rocks intercalated with mudstone, siltstone, and impure limestone. The massive sulfides are located immediately above the impure limestone unit. The hangingwall of the massive sulfides is formed by a ~100-m-thick unit dominated by felsic volcanic rocks and polymict breccias and a ~200-m-thick, relatively homogeneous crystal-rich volcanoclastic unit (Polliand and Fontboté, 2000; Polliand et al., 2005). Coherent rhyolite units in the immediate footwall and hangingwall of the massive sulfides yielded U-Pb zircon ages of  $69.71 \pm 0.18$  Ma and  $68.92 \pm 0.16$  Ma, respectively (Polliand et al., 2005). Similar to Cerro Lindo, the massive sulfides at Perubar and their host rocks have been subject to contact metamorphism caused by the intrusion of the Peruvian Coastal batholith (Polliand et al., 1999).

In addition to Perubar, several other VMS deposits in the Cañete regions appear to be hosted by Maastrichtian to Danian (~69-63 Ma) submarine volcanic rocks. This may include the Aurora Augusta and Balducho deposits located near Lima (Romero, 2007). The Aurora Augusta deposit has produced approximately 150,000 tons of barite since 1975 and is known to be host to a small polymetallic sulfide zone hosted by strongly silicified volcanic rocks (Vidal, 1987; Steinmüller et al., 2000). The hangingwall of the deposit is composed of andesitic volcanoclastic rocks interbedded with vesicular lavas (Vidal, 1987). The Balducho deposit is comprised of barite and pyrite-sphalerite lenses hosted in slate and hornfelsic graywacke within the contact metamorphic aureole of an intrusions belonging to the Coastal batholith (Vidal, 1987).

### **1.3. Deposit Stratigraphy**

The Palma VMS deposit is located ~50 km east of Lima in Lurín Valley (Fig. 1.2, 1.3). The massive sulfides of the Palma deposit are hosted by a succession of submarine sedimentary and volcanic rocks forming part of the up to ~600-m-thick Quilmaná Formation (Vidal, 1990). No

geochronological work has been conducted on the host rocks of the Palma deposit so far and it is, therefore, unknown whether the Quilmaná Formation is part of the late Albian to Turonian Casma Group or formed during the younger Maastrichtian to Danian episode of submarine volcanism and sedimentation. Based on lithological similarities, the Quilmaná Formation may be correlative to the Maastrichtian to Danian host rock succession of the nearby (~20 km) Perubar deposit (Noble et al., 2005).

As part of the present study, eight exploration drill holes totaling 2,300 m of core were logged graphically to study the distribution of sedimentary and volcanic facies within the Quilmaná Formation at Palma. Combined with routine logging of ~40 km of exploration core and property mapping by Volcan Compañía Minera, the Quilmaná Formation was subdivided into four informal members (Fig. 1.4, 1.5). Primary sedimentary and volcanic textures are generally well preserved at Palma, allowing the use of primary rock nomenclature.

The Palma Basalt member represents the lowest stratigraphic unit recognized at the Palma deposit. It has a minimum thickness of ~110 m. The base of the Palma Basalt member has not been intersected by exploration drilling and has also not been recognized during property mapping. The lower part of the Palma Basalt member is dominated by massive basalt containing intercalated carbonaceous mudstone units. The abundance of basalt units decreases gradually towards the top of the member where carbonaceous mudstone forms the most abundant rock type. The massive sulfides of the Palma deposit are hosted largely within the upper part of the Palma Basalt member.

The carbonaceous mudstone of the Palma Basalt member has been intruded by mafic units forming a sill and dike complex. The mafic units are aphyric or porphyritic and typically sharp contacts with the enclosing carbonaceous mudstone. The mafic units were affected by hydrothermal alteration and contact metamorphism related to the Coastal batholith. Contact metamorphism resulted in the formation of abundant biotite (Fig. 1.6). The color of these mafic rocks varies from dark brown to dark greenish. Plagioclase is typically altered to secondary phases although faint feldspar laths can be identified in some cases in hand specimen.

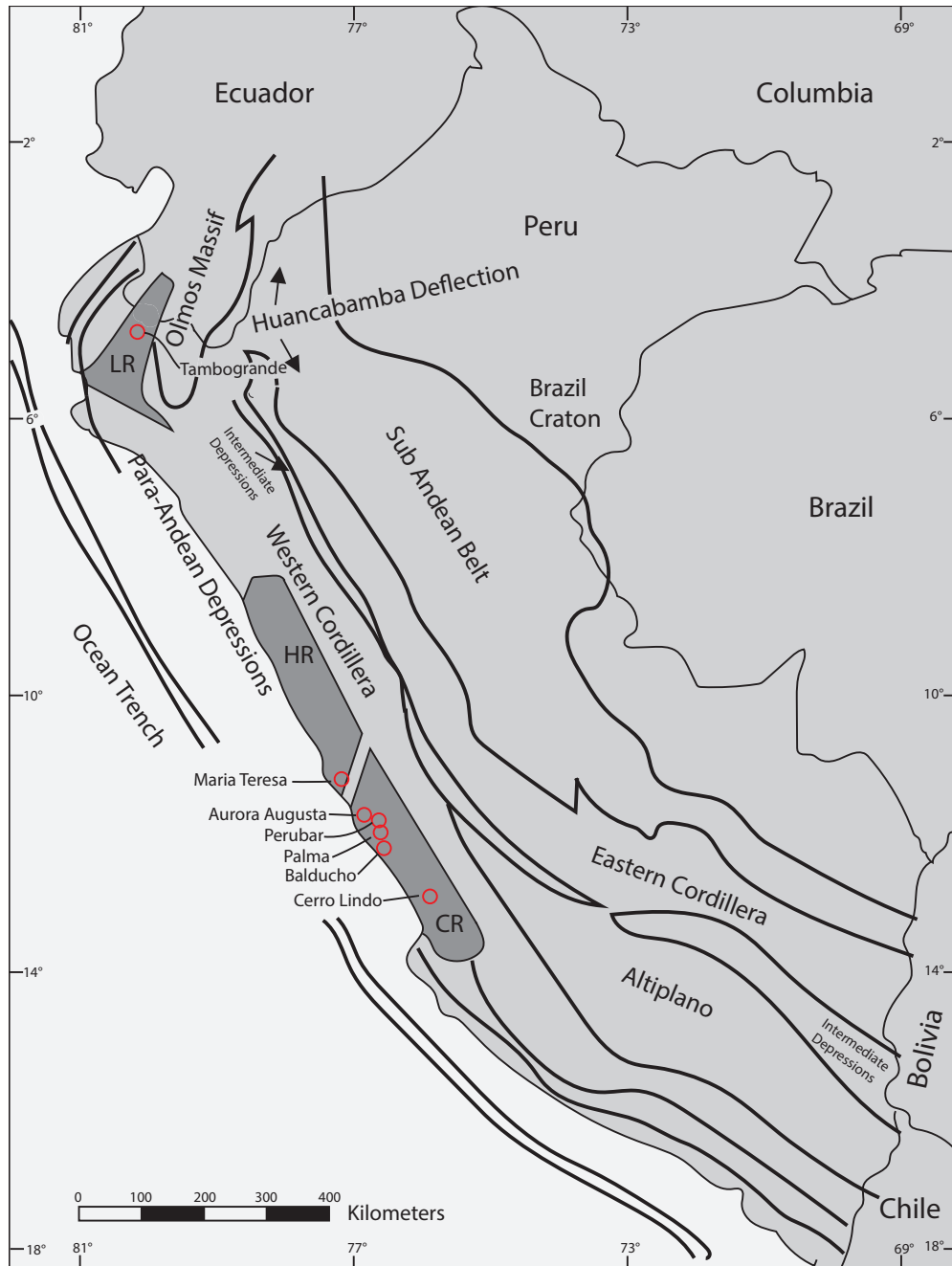


Figure 1.1. Morphostructural units of the Peruvian Andes. Outcrop areas of the Cretaceous submarine volcanic and sedimentary rocks. Also shown are the locations of major VMS deposits (modified from Benavides-Cáceres, 1999). CR = Cañete region, HR = Huarney region, LR = Lancones region.

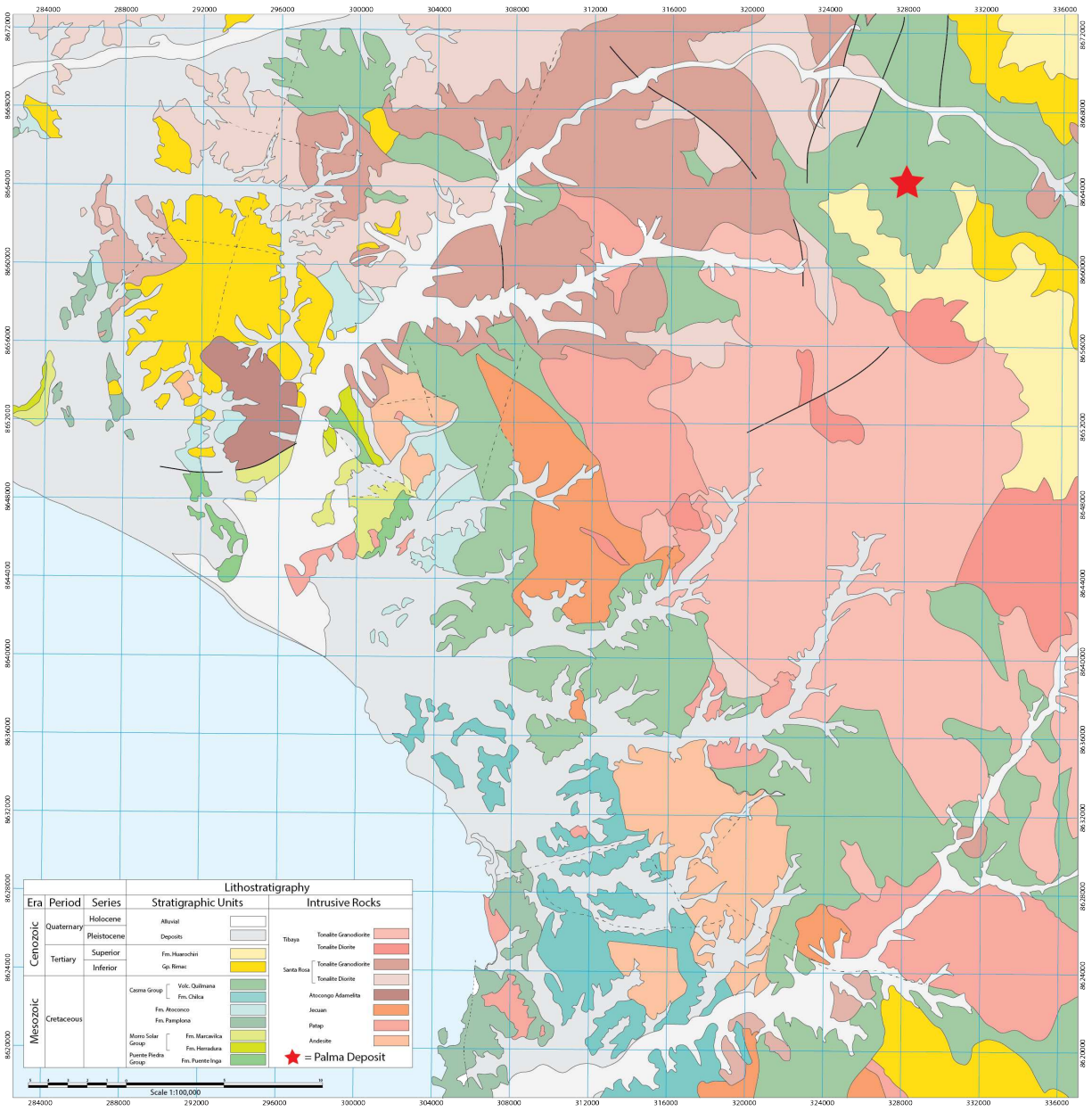


Figure 1.2. Geological map of the region southwest of Lima showing the outcrop area of Cretaceous submarine volcanic and sedimentary rocks and the location of the Palma deposit (modified from León et al., 2002).

In the upper part of the Palma Basalt member, many of the mafic units have contacts with the enclosing carbonaceous mudstone that are marked by the occurrence of mudstone-matrix breccias formed through the mixing of the lava and the host sediment (Fig. 1.6). The contact relationships are complex in detail involving intricate interpenetration of the lava and the sediment. Bedding in the sediment is commonly destroyed or contorted. The mudstone close to the contact with the basalt clasts is indurated and commonly silicified. The basalt clasts vary from angular and blocky to lenticular, bulbous, or lobate. The basalt is commonly chilled along the contact with the carbonaceous mudstone matrix. Basalt units mantled by mudstone-matrix breccias are particularly common towards the top of the Palma Basalt member, but never occur within the uppermost tens of meters.

The Palma Basalt member is conformably overlain by the Palma Marker member. This unit is on average ~20 m in stratigraphic thickness and is composed of variably altered and bleached mudstone. Individual mudstone layers are ~10 cm in thickness and range from dark black, brown to light grey. The mudstone is variably silicified. Some layers are brecciated due to the high abundance of carbonate veins. The mudstone contains bands that contain 70–90 % diopside porphyroblasts set in a white-light grey mudstone matrix (Fig. 1.6). The diopside porphyroblasts range up to ~1 mm in size. The layers containing abundant diopside porphyroblasts are commonly parallel to bedding, but pinch and swell resembling bedding-parallel alteration. The fine-grained rocks of the Palma Marker member generally lack pyrite or other sulfide minerals. The Palma Marker member is host to some mafic intrusions characterized by the presence of abundant metamorphic biotite.

The Palma Marker member is conformably overlain by the Palma Pelite member. This member comprises ~700 m of carbonaceous mudstone (Fig. 1.6). Optical microscopy shows the mudstone is composed dominantly of fine-grained detrital quartz and feldspar grains set in a matrix that is rich in mica and organic material. The mudstone of the Palma Pelite member is macroscopically unaltered although silicification is locally present. Small carbonate veins are abundant that are interpreted to be of metamorphic origin. Only few mafic rocks containing biotite were recognized in this stratigraphic position.

The Palma Pelite member is conformably overlain by the Palma Limestone member. In weathered outcrops, the limestone of this member has a light gray appearance and can be easily identified. Because of the high carbon content, hand specimens of the limestone tend to be black and appear to be fine-grained to slightly granular. In thin section, the limestone is primarily composed of calcite (~85%). The organic material occurs as elongate wispy domains.

The host rocks of the Palma deposit form the eastern limb of an open, drag-folded anticline. The fold axis of the anticline plunges to the southeast. In outcrop, bedding of the Palma Marker member strikes  $077^{\circ}$  and dips  $45^{\circ}$ . There are three major faults that transect the stratigraphy. This includes a NE-striking normal fault, a N-striking reverse fault, and a NW-striking strike-slip fault with a sinistral movement that displaces mineralization by ~90 m (Fig. 1.3).

All members of the Quilmaná Formation are crosscut by late phaneritic dikes that are dioritic or gabbroic in composition. The dikes have not been affected by hydrothermal alteration and feldspar and ferromagnesian phases in these units can be readily identified in hand specimen. The mafic dikes vary from light grey to green in color and commonly exhibit chilled margins. In addition, subordinate amounts of porphyritic dikes occur that are more felsic in composition. The dikes have apparently not been overprinted by the contact metamorphism related to the emplacement of the Coastal batholith and are probably Neogene in age. They may represent feeder dikes to the Miocene Huarochiri Formation, which represents the youngest stratigraphic unit exposed in the Palma area. This formation unconformably overlies the host rock succession of the Palma massive sulfide deposit. The Huarochiri Formation consists of sedimentary and volcanic rocks, including andesitic tuffaceous rocks and trachyandesite. The rocks of this formation partly cover the host rock stratigraphy along strike to the southwest of the deposit area (Fig. 1.3).

#### **1.4. Ore Zones**

Initial work at Palma commenced in 1985. Following mapping, surface sampling, and diamond drilling, a small mining operation was set-up processing ~90 tons of ore per day. A total of 1,700 m underground development was conducted. At the time, a total resource of 134,000

tons grading 9.45 wt. % Zn and 2.38 wt. % Pb was defined. Based on more recent drilling, an inferred resource of 5.590 million tons grading 7.43 wt % Zn, 1.50 wt % Pb, and 44.1 g/t Ag was defined in 2017 (Volcan Compañía Minera Reserves and Resources 2017).

The Palma deposit comprises a conformable ore zone that is hosted by the upper part of the Palma Basalt member. This zone is rich in Zn, Pb, and Ag, but has low overall Cu grades. The ore envelop is up to 125 meters in thickness, but includes a large number of smaller parallel ore lenses separated by the early mafic sills. Individual lenses range from 1-13 m in thickness (Fig. 1.7) and can range in base metal grade from 4% sphalerite and 1% galena up to 50% sphalerite and 11% galena. The ore zone can be followed down dip for ~620 m. Although continuity has not been proven yet, sulfide mineralization can be traced over a strike length of ~2.5 km (Volcan Compañía Minera Annual Report 2016), possibly suggesting that the deposit is much larger than indicated by the current inferred resource. The conformable ore zone at Palma is dissected by faults and fault repetitions have been noted in six of the eight drill holes logged as part of the present study. In addition, it is important to take into account that the Miocene intrusions crosscutting the conformable ore lens cause significant dilution, which is estimated to be on the order of ~30 percent.

The ore in the conformable sulfide zone is entirely hosted by the mudstone of the Palma Basalt member and occurs as massive sulfide replacing the previously carbonate-altered mudstone. The ore is primarily composed of pyrite, sphalerite ranging in composition from ZnS to  $Zn_{0.87}Mn_{0.13}S$  and  $Zn_{0.73}Fe_{0.2}Mn_{0.07}S$ , as well as pyrrhotite with lesser galena PbS and minor chalcopyrite. Silver is contained in achucchacuite  $AgMnPb_3Sb_5S_{12}$ . The textural characteristics of the sulfides are described in more detail below.

Recent drilling has identified a discordant zone of sulfide mineralization that is located stratigraphically deeper in the volcanic succession. Sulfides in this zone occur as stringers, irregular patches, or disseminated grains. The discordant sulfide zone is predominantly hosted in intensely altered mafic rocks although mudstone intervals separating the mineralized and intensely altered mafic units can be replaced by sulfides. The discordant sulfide zone primarily consists of pyrrhotite with localized concentrated chalcopyrite. The grades range up to 2.64% Cu

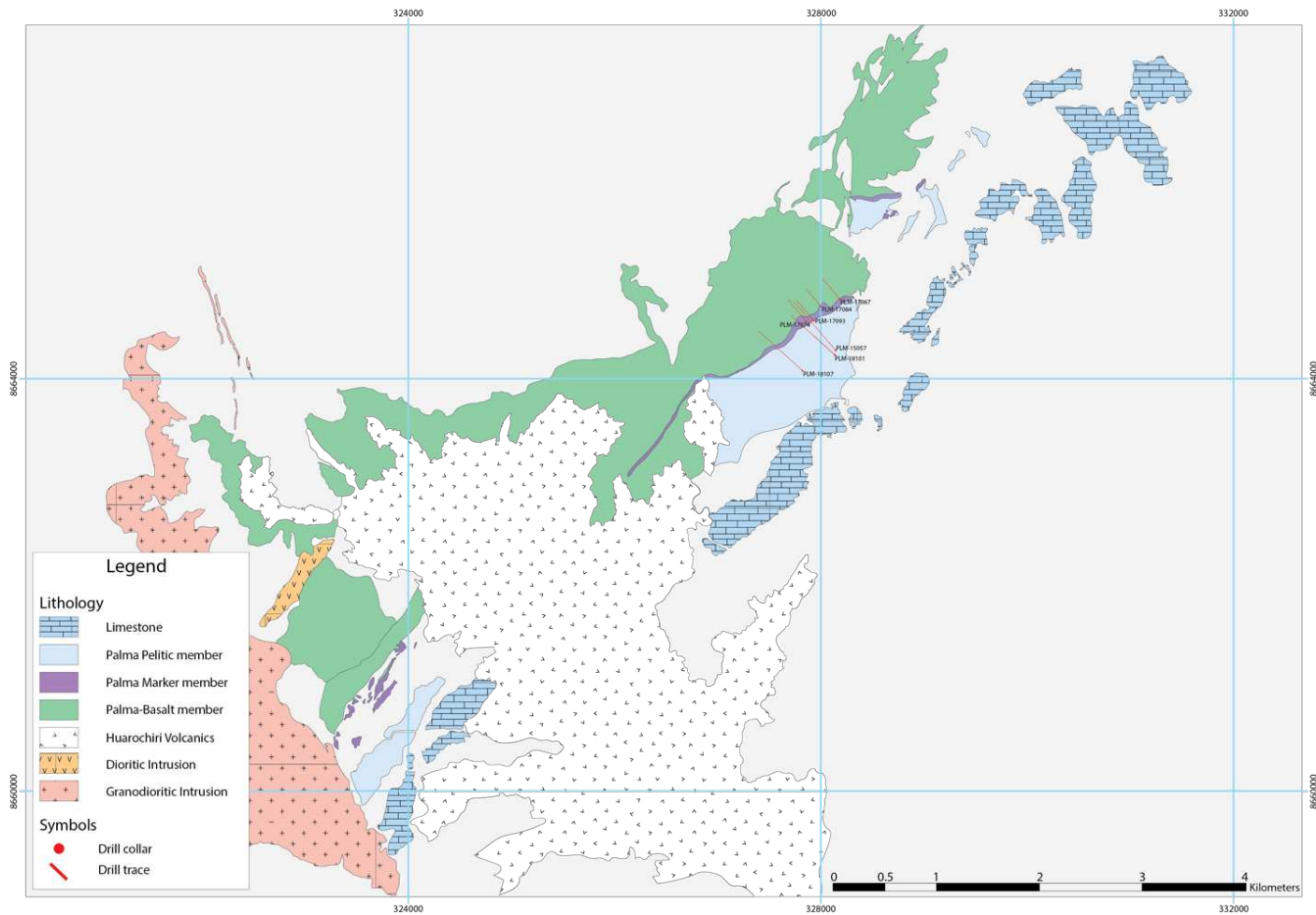


Figure 1.3. Geological map of the Palma deposit area showing the distribution of the different members of the Quilmaná Formation.

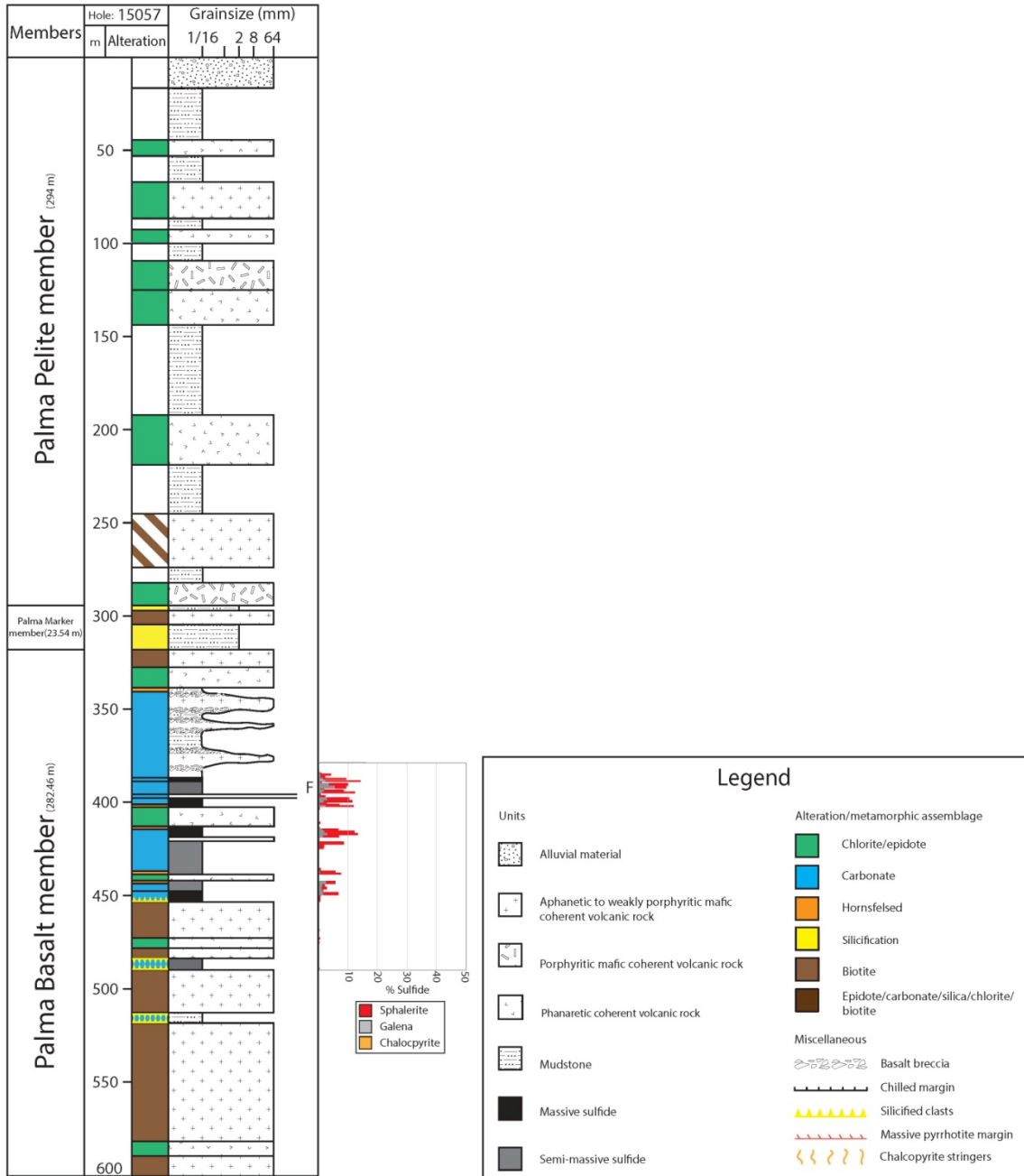


Figure 1.4. Graphical log of drill core 15057 that intersected the entire host rock stratigraphy of the Palma deposit. The graphic log illustrates the stratigraphic relationships and the abundance of mafic dikes and sills in the sedimentary host rock succession

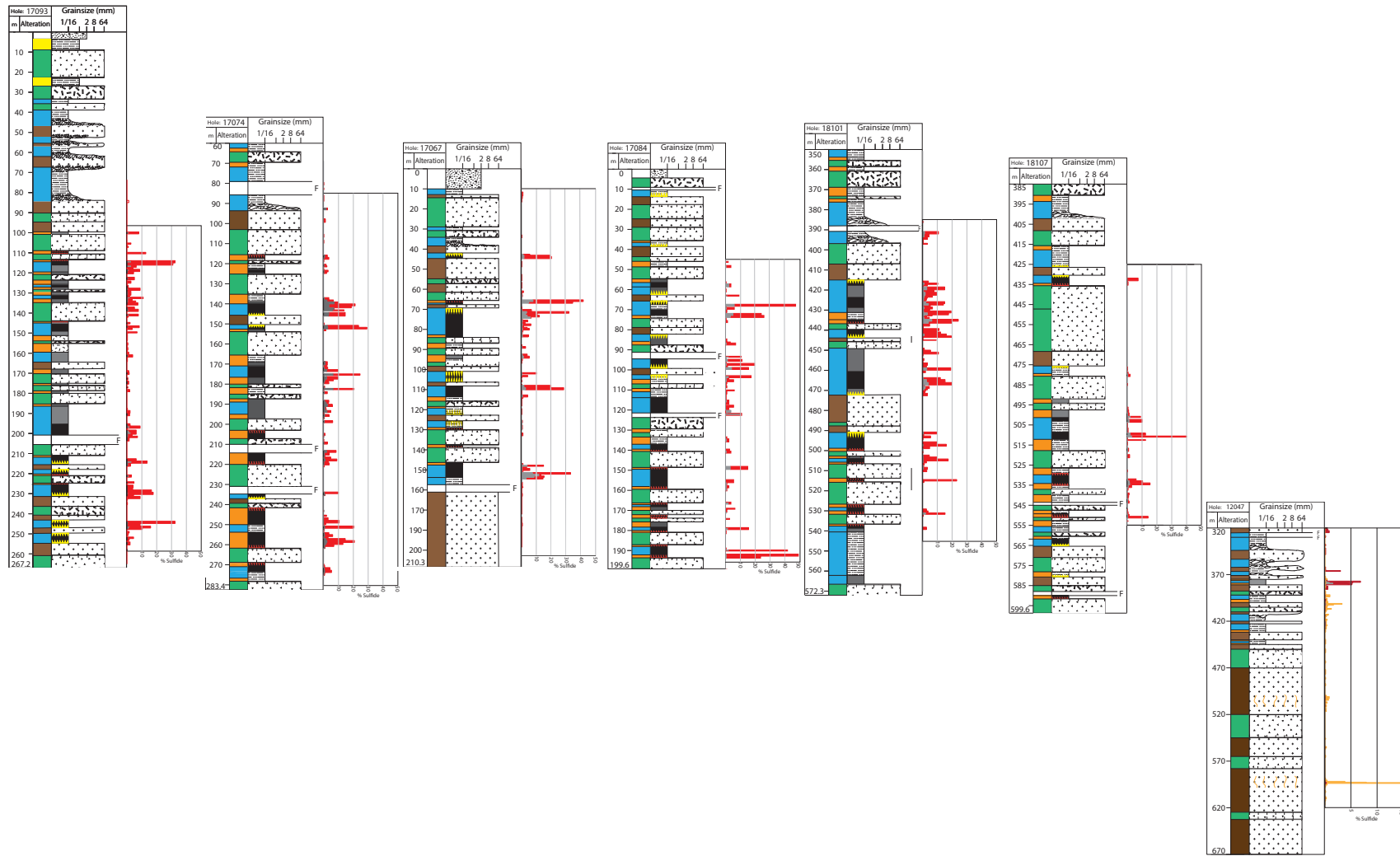


Figure 1.5. Graphical logs of drill holes intersecting parts of the host rock stratigraphy of the Palma deposit.

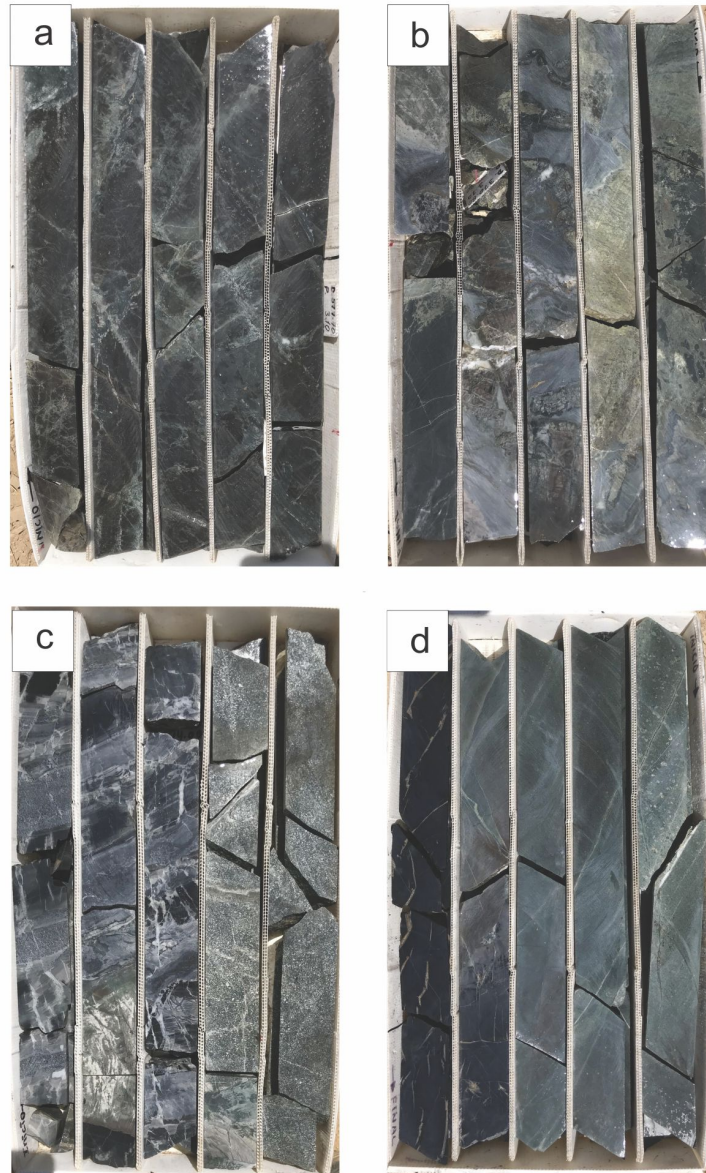


Figure 1.6. Photographs of representative drill core from the host rock succession of the Palma deposit. a. Biotite-bearing basalt of the Palma Basalt member. b. Peperitic margin of a shallow intrusion in the Palama Basalt member that is hosted by a carbonaceous mudstone. c. Silicified mudstone of the Palma Marker member that contains abundant diopside porphyroblasts. The sedimentary deposit is cut by a late mafic dike. d. Unaltered mudstone of the Palma Pelite member that is cut by a dike containing only small amounts of biotite.

over intersections of ~2.5 meters width. In the mafic rocks, the discordant sulfide mineralization is surrounded by ~100 m of a distinct patchy epidote-silica-chlorite-carbonate alteration. Epidote alteration occurs as larger patches up to 1 m, with intensely disseminated sulfide, as well as islands in the sulfide-rich patches. The silica is creamy and white occurring as large patches with epidote, or as disseminated irregular blebs in the biotite-chlorite-altered sections. Chlorite occurs as fine-grained patches associated with fine-grained, patchy biotite.

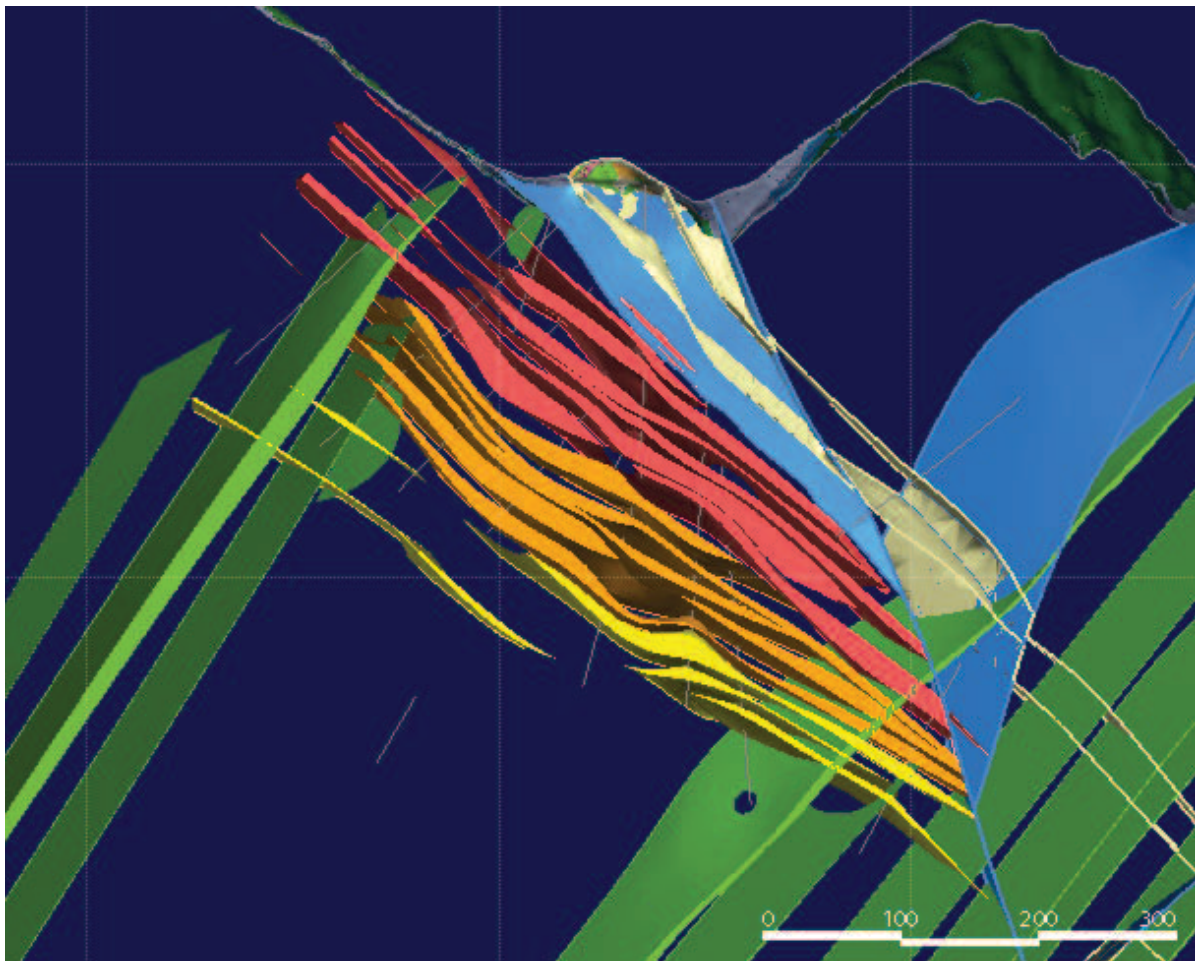


Figure 1.7. Cross-section of through the Palma deposit constructed using the advanced 3D modeling software Leapfrog. The massive sulfide lenses separated by mafic sills are given in red, orange, and yellow colors. The surface is given in grey and a crosscutting faults are given in blue and green.

## 1.5. Gangue and Ore Textures

### 1.5.1. Carbonate textures

Intense carbonate alteration occurs in the upper part of the Palma Basalt member stratigraphically above the conformable massive sulfide zone. A variety of carbonate textures can be observed throughout this ~170-m-thick stratigraphic interval. The carbonate minerals, mostly calcite, form a cement in the matrix of the mudstone. The mudstone is black, and extremely fine-grained (Fig. 1.8a). The ratio of mudstone to calcite, as well as the shapes, sizes, orientations, and rheology of mudstone vary. Those textures are described below. The description focuses on textural end-members although different textures commonly occur over distances of only several centimeters.

*Wispy, banded calcite containing milled sediment and irregular mudstone clasts:* This texture occurs throughout the carbonate-altered mudstone and commonly forms the matrix to other textural alteration types. In hand sample, the mudstone is light to dark grey, with a speckled, fuzzy texture. It occurs as delicate, wispy, sub-millimeter to centimeter-scale bands. The color differences between bands are dictated by the sediment to calcite ratio, the more mud the darker. The wispy bands have orientations dictated by the surrounding material (Fig. 1.8b). The bands drape, and wrap around fragments of mudstone (Fig 1.9a), and are parallel to beds of mudstone and contacts with biotite-altered basalt.

In thin section, the calcite grains are elongated with angular to sub-rounded pieces of mudstone suspended in the carbonate. In bands with a higher proportion of <1 mm mudstone fragments, pull-apart and slump microstructures can be seen in the irregularly-shaped mudstone clasts (Fig. 1.9a). There are also irregular-shaped grains of pyrite containing cores of mudstone. In the mudstone masses, there are elongated, sometimes interconnected channels of calcite, causing some masses to appear laminated (Fig 1.9b). The margins of mudstone clasts to calcite are fuzzy, with extremely fine-grained sediment being contained in the calcite.

*Laminations of calcite in laminated mudstone:* This texture appears in almost all textural variations. In hand sample, it appears as a black laminated mudstone with mm-scale, light grey laminations (Fig. 1.8a). In thin section, it appears as a laminated mudstone, with preferentially oriented, elongated, interconnected bands of micro-sparry, fibrous calcite (Fig 1.9a).

*Alternating laminated mudstone bands and wispy calcite-mud bands:* This texture consists of bands of relatively continuous mudstone, alternating with bands of wispy calcite and sediment. The bands are fairly uniform in thicknesses, alternating between the wispy, calcite-mud bands, and laminated mudstone bands (Fig. 1.8d). The laminated mudstone bands are often broken up by the wispy calcite-mud. In some instances, the mudstone bands are fractured, creating a clast-supported, angular mudstone breccia. The crosscutting carbonate forms a matrix in the mudstone bands that is much lighter grey, with less sediment than the wispy calcite-mud bands. At cracks in the mudstone, the darker, banded wispy calcite-mud appears to swell into the lighter calcite matrix in the laminated bands of mudstone (Fig. 1.8e). The wispy calcite-mud bands also swell into the mudstone bands, crosscutting the laminations (Fig. 1.8d).

*Matrix-supported, mudstone breccia:* This monomict mudstone breccia varies in clast size and shape. The clasts can be laminated, rectangular and blocky (Fig. 1.8f) or irregularly shaped in a banded wispy calcite-mud matrix. The clasts can be concentrated along the same plane, or distributed more randomly (Fig. 1.8g). The laminations in the mudstone clasts are either the same orientation as the wispy carbonate bands (Fig. 1.8f), or are tilted and turned, suggesting clast rotation. In many cases, the clasts occurring along individual bands form a jigsaw and could be fit together. However, the clasts can also be rotated and slightly rounded.

*Clast-supported, mosaic, mudstone breccia:* This monomict mudstone breccia appears in two variations. One contains angular, blocky clasts of jigsaw fit mudstone clasts in a calcite-mud matrix (Fig. 1.8h). The second variation has irregular-shaped clasts with curved margins (Fig. 1.8i). This variation is also jig-saw fit with a wispy calcite-mud matrix.

*Contorted, curved, continuous bands of mudstone in wispy calcite-mud matrix:* In this textural type, the banded mudstone behaves more ductile, than the previous cases. The bands are

laminated, but instead of breaking into clasts, the laminations are bent and contorted (Fig. 1.8j). The laminations are also curved. These bent, contorted bands are completely surrounded by the dark wispy calcite-mud. In some areas, the mudstone is broken or cracked and filled in with calcite. This texture occurs at the scale of 6 cm beds, to 2 mm bands of mudstone, and resembles soft sediment deformation.

*Ellipsoidal impregnations in mudstone:* In this variation, the wispy calcite-mud forms ellipsoidal, impregnations in laminated mudstone. These impregnations swell, and crosscut laminations in the mudstone. They seem to cause minor displacement in the mudstone clasts, appearing to give an inflating effect to the bedded mudstone (Fig. 1.8k).

*Wispy banded calcite without mud:* This texture is visually similar to the *Wispy, banded calcite containing milled sediment and irregular mudstone clasts*, but appears more white as it lacks sediment. This texture occurs in contact with aphanitic basalt. The wispy bands often occur perpendicular to the intrusive contact. This texture occasionally has rafts of the mafic material, with tapered tails at the same orientation as the bands in the calcite (Fig. 1.8l).

### **1.5.2. Silicified textures**

Silicification occurs at the margins of biotite-altered basalt and mudstone in the upper part of the Palma Basalt member. Silicified mudstone clasts show sub-millimeter-thick laminations that are identical to those observed in unaltered mudstone. However, the silicification has resulted in color changes with individual laminations ranging from light grey-white to dark grey or light pink to brown-grey. The silicified clasts are generally not rotated although individual clasts may be separated by a finer-grained matrix. The clasts have been affected by both ductile and brittle deformation. The clasts show curved laminations and bands or may be blocky and angular. The matrix wrapping around the clasts is commonly also silicified.

Figure 1.8. Core photos of carbonate-altered mudstone. a. Relatively unaltered laminated mudstone. b. Wispy banded calcite with incorporated sediment. c. Wispy banded calcite draping around large mudstone masses. d. Alternating laminated mudstone and wispy calcite-mud bands. Wispy calcite-mud swells into mudstone bands. e. Low mud/calcite ratio in cracks of mudstone bands with higher mud/calcite ratio swelling into cracks. f. Matrix-supported monomict mudstone breccia with blocky, rectangular, and oriented clasts. g. Matrix-supported monomict mudstone breccia with irregular-shaped clasts. h. Clast-supported monomict mudstone breccia with angular blocky clasts. i. Clast-supported monomict mudstone breccia with irregular shaped clasts with curved margins. j. Contorted, curved mudstone band with curved laminations. k. Ellipsoidal impregnations of wispy calcite-mud in mudstone. l. Banded calcite lacking sediment wrapping around basalt clasts.

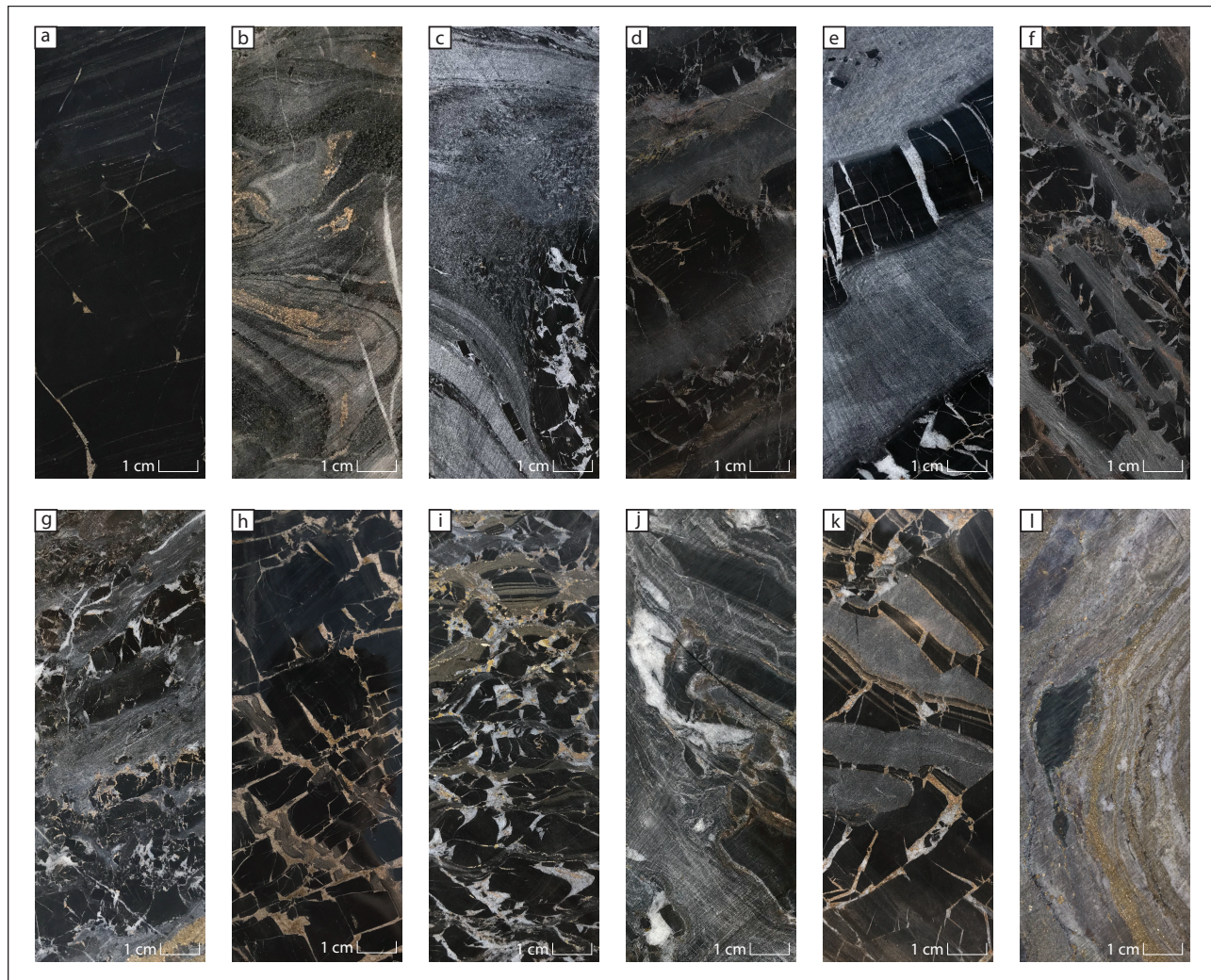
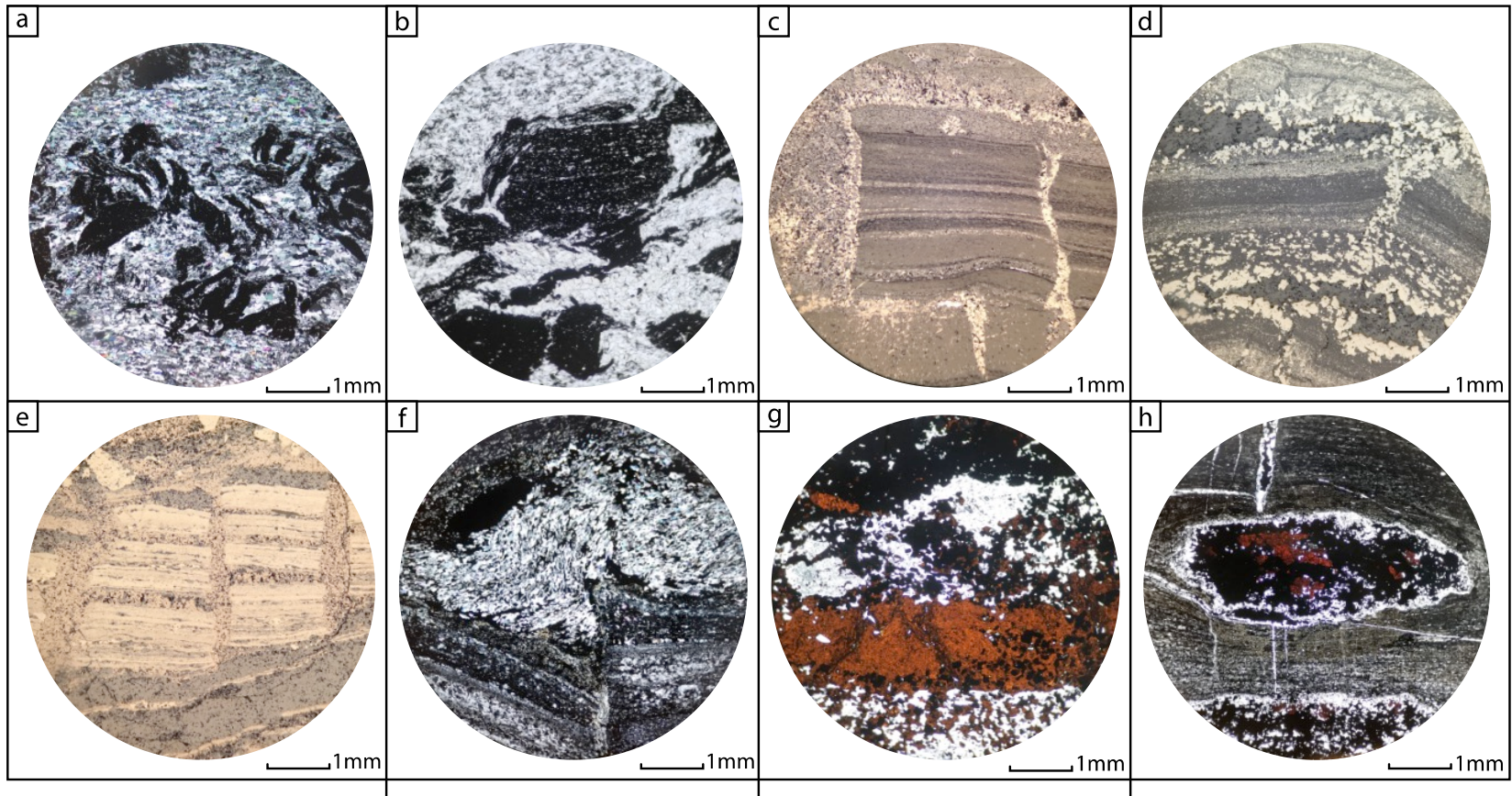


Figure 1.9. Microphotographs of carbonate-altered mudstone, carbonate-sulfide-altered mudstone, and sulfide-altered mudstone. a. Plain-polarized light image of carbonate-altered mudstone. The mud forms wispy domains in the carbonate matrix and exhibits pull-apart textures. b. Plain-polarized light image of a carbonate-altered mudstone containing mudstone clasts in the calcite matrix. c. Reflected light image of pyrite occurring along laminations in a mudstone clast. d. Reflected light image of a mudstone clast containing more pyrite along the laminations. e. Reflected light image of a mudstone clast that is almost entirely replaced by pyrite. f. Crossed-polarized light image showing elongated calcite grains with minor pyrite wrapping around a mudstone clast. g. Plain-polarized light image of a wispy band of calcite and mudstone containing a high content of sphalerite, which appears dark red in transmitted light. h. Plain-polarized light image of a mudstone clast that is replaced by sphaerite and pyrite. The clast is rimmed by calcite.



### 1.5.3. Sulfide textures

The sulfide textures observed in core are essentially identical to those occurring in carbonate-altered mudstone (Figs. 1.9 and 1.10). Observations in drill core suggest that sulfide formation occurred through replacement of the earlier formed carbonate. Sulfide intervals in core range from semi-massive to massive. The wispy calcite-mud matrix in ore samples is partially to completely replaced and only traces of carbonate may be left (Fig. 1.9f-g) The mudstone clasts and beds range from few sulfide laminations to near complete sulfide clast replacement (Fig. 1.9c-e). As opposed to rehearsing the textures described above, only wispy calcite-mud with sulfide and carbonate altered mudstone with sulfide are described below.

*Wispy calcite-mud matrices with sulfide:* In hand sample, the calcite-mud matrices are preferentially oriented, forming around mudstone and biotite-altered basalt. In thin section this appears as elongated, preferentially oriented calcite grains (Fig. 1.9f). A majority of the matrices contain sediment. The matrix occurs as infill in clast and matrix supported breccias (Fig. 1.10d-e), bands between beds of mudstone (Fig. 1.10b), as well as large sections of wispy calcite material (Fig. 1.10i). Pyrite, pyrrhotite, sphalerite, galena, and uchucchacuite all occur in the banded calcite in varying proportions. In thin section, the wispy bands are compositionally distinct, with varying amounts of sulfide, carbonate, and detrital material. In variations with less sulfide, thin sections are predominately composed of recrystallized calcite (Fig. 1.9f), with concentrated sub-millimeter to centimeter-scale bands of irregular sphalerite and recrystallized to blebby pyrite. The pyrite occurs separately or as inclusions in sphalerite. Galena occurs as portions of larger, irregular-shaped sphalerite grains (Fig. 1.11c). Uchucchacuite occurs as microscopic inclusions in sphalerite (Fig. 1.11b). As the sulfide proportion increases in these textures, the pyrite and sphalerite tend to form skeletal, interconnected networks to patches (Fig. 1.9g). The patches usually have islands of quartz grains, calcite, and other sulfides. As sulfide abundance increases, calcite abundance decreases.

*Carbonate-altered mudstone with sulfide:* In hand sample, this texture appears as laminated, alternating mm-scale bands of dark siliciclastic mud and light grey-colored bands. In thin section the calcite grains are preferentially oriented, and elongated occurring in semi-interconnected,

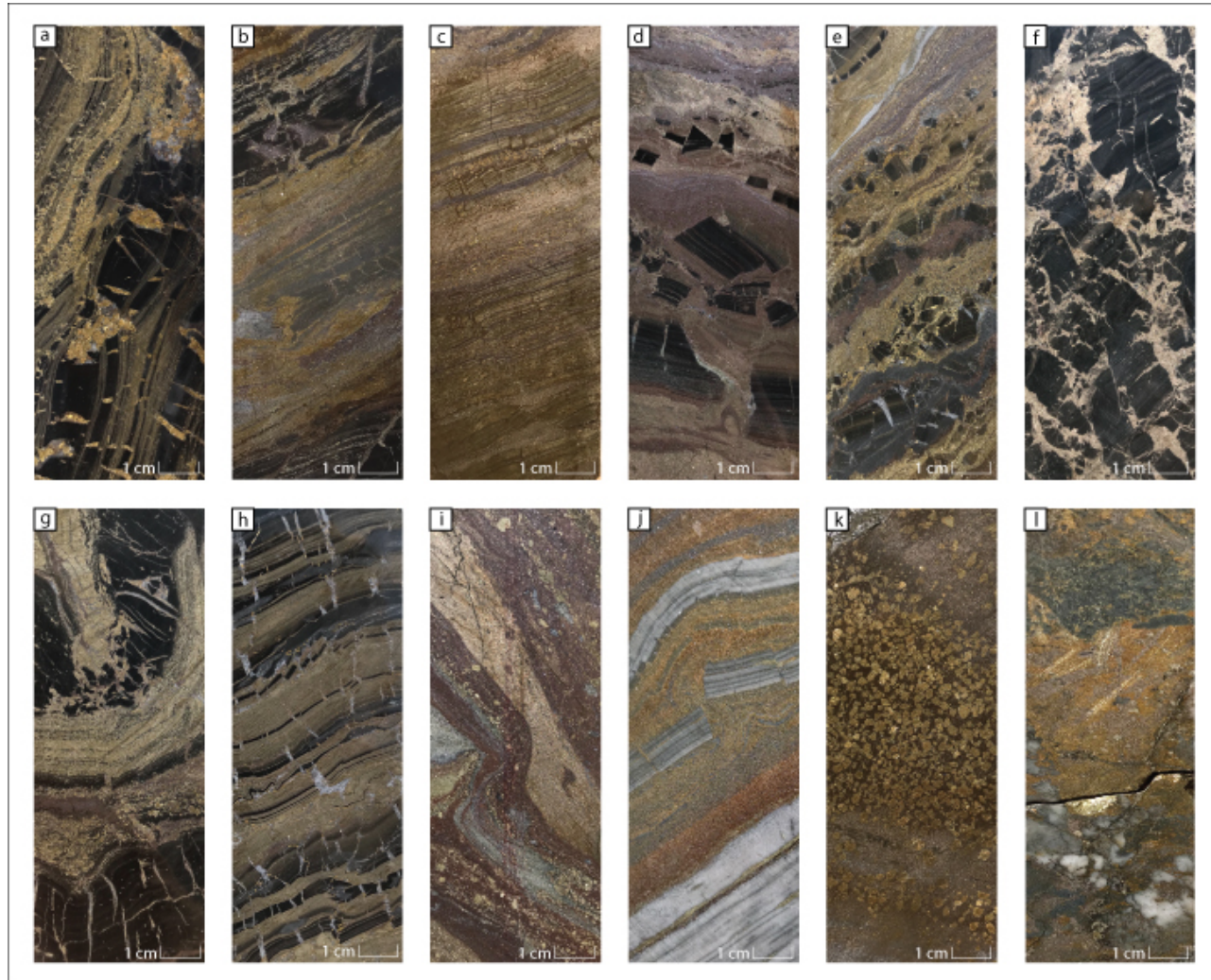
concentrated bands. This texture also occurs in all sulfide-containing laminated mudstone textures. The dominant sulfide in these laminations is pyrite. It takes on the same texture as the carbonate as concentrated bands, of elongated to sub-rounded pyrite grains in a laminated mudstone clast (Fig 1.9c-d). This can occur with carbonate and minor pyrite to almost pyrite in laminated mudstone with no carbonate almost complete pyrite (Fig. 1.9e). The more pyrite, the more interconnected the networks of pyrite become. In the clasts that are almost completely replaced by pyrite, the pyritic bands occur with intergrowths of pyrrhotite with disseminations of galena (Fig. 1.11d). They also have inclusions of elongated, oriented islands of sediment with sphalerite. Sphalerite also appears as disseminations to interconnected disseminations in the pyrite, but on a very small scale. Sphalerite usually occurs in clasts as infill of ellipsoidal impregnations in the mudstone (Fig. 1.9h), but occasionally occurs as laminations with islands of pyrrhotite (Fig. 1.9a).

## **1.6. Contact metamorphic overprint**

The Palma deposit is located ~4 km northeast of a large granodiorite belonging to the Coastal batholith. The intrusion resulted in the contact metamorphic overprint of the massive sulfides and their host rock succession (Fig. 1.12).

Mafic volcanic rocks of the Palma Basalt member contain abundant biotite that is interpreted to be of metamorphic origin. The biotite is usually Mg-rich with a formulae derived from semiquantitative energy-dispersive X-ray fluorescence analysis of  $K(Mg_{1.75}Fe_{1.09})Ti_{0.16}Al_{1.3}Si_{2.69}O_{10}(OH)_2$ . The biotite varies in composition and can have elevated Fe contents, with a formula of  $K(Mg_{1.5}Fe_{1.5})Al_{1.43}Si_{2.57}O_{10}(OH)_2$ . Microscopically, the biotite occurs as networks around islands of pure albite with anorthite rims. The biotite occurs homogeneously throughout the mafic units. However, locally the biotite is more patchy and crosscut by <2 cm wide zones of fine-grained patchy, dark green chlorite. These zones of chlorite may be of retrograde origin. In addition, the biotite overprint also occurs on the epidote-silica-carbonate-chlorite alteration assemblage associated with the sulfide stringers.

Figure 1.10. Core photos of sulfide textures. a.) Sulfide laminations in mudstone that curved with ellipsoidal impregnations of sulfide b.) Alternating laminated mudstone bands with sulfide dominant bands. c.) Full sulfide clast replacement. d.) Pseudo-banded monomict, matrix-supported mudstone breccia. Clasts are blocky and experience partial sulfide replacement and matrix experiences near full sulfide replacement. Clasts have dimensions that fit together but are slightly displaced. e.) Mudstone clasts are irregular, with multiple orientations. Clasts experience partial replacement and matrix experiences near full replacement. f.) Clast-supported monomict breccia with irregular shaped clasts and a sulfide matrix. g.) Contorted, curved bands of mudstone with curved laminations in wispy sulfide matrix. h.) Bands of mudstone exhibit ductile and brittle rheologies. i.) Flow-y banded sulfide-calcite with no detrital mud at contact of heavily altered intrusion. j. Silicified, laminated mudstone in sulfide matrix. Sulfide minerals occur as a wispy banded matrix wrapping around clasts and in cracks and laminations in silicified clasts. The clasts show ductile and brittle behavior. k. Massive pyrrhotite grading into euhedral, recrystallized pyrite in a pyrrhotite matrix. l. Chalcopyrite stringers.



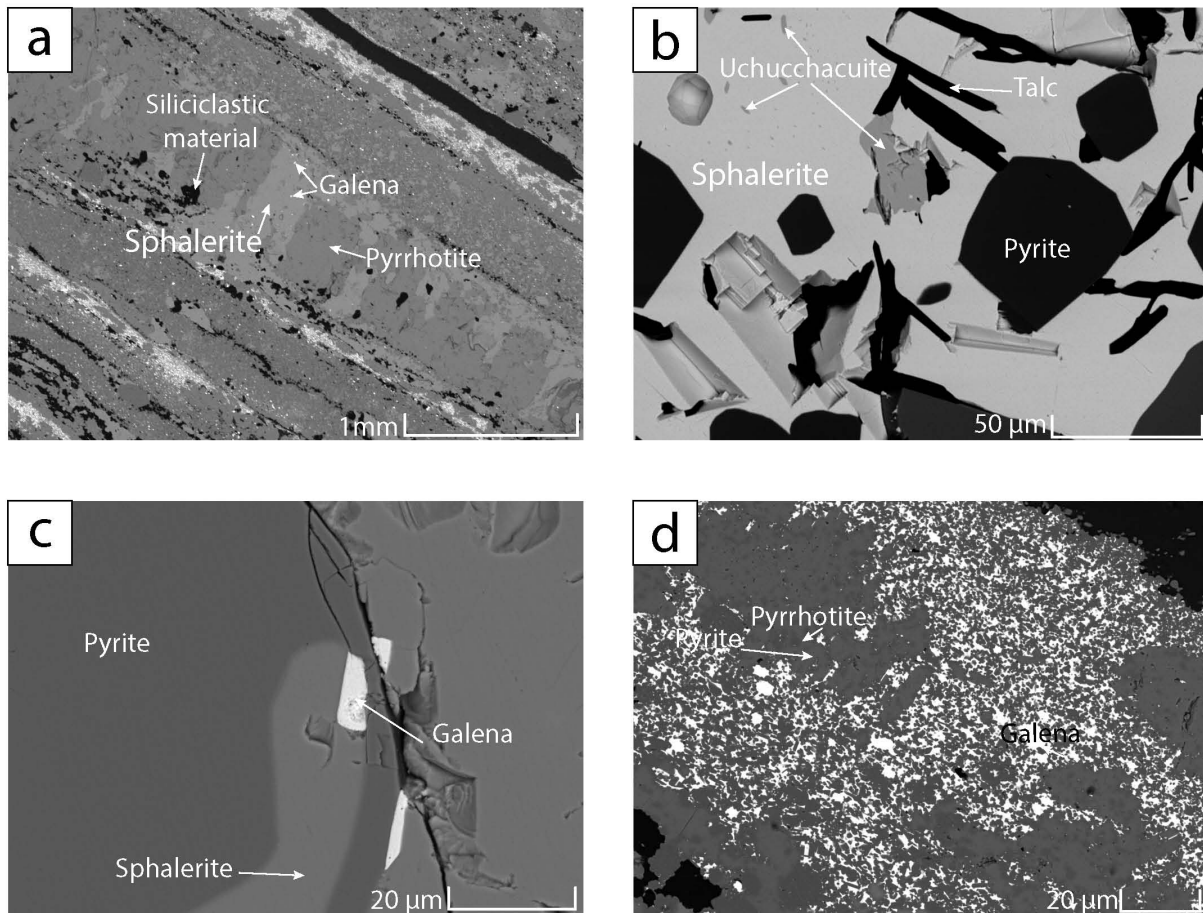


Figure 1.11. Backscattered electron images of sulfide textural relationships. a. Lamination of former mudstone that is entirely replaced by sulfide minerals. b. Uchucchacuite forming an inclusion in sphalerite that is intergrown with pyrite and talc c. Galena inclusion in an irregular, blebby sphalerite grain. The sphalerite is surrounded by pyrite. d. Intergrowth of pyrite and pyrrhotite in a lamination of the former mudstone that is fully replaced by sulfide minerals. Galena occurs in trace concentrations.

The metamorphic overprint of the ore zones resulted in recrystallization of the massive sulfides. Pyrite, pyrrhotite, sphalerite, and galena in the ore are coarse grained forming large interlocking grains. The sulfide grains commonly reach up to 1 mm in size. Grain coarsening has also occurred in carbonate-altered rocks. The carbonate minerals in zones of intense hydrothermal alteration are granoblastic and coarse-grained.

The most obvious effect of the metamorphic overprint of the host rock succession is the occurrence of the diopside porphyroblasts in the mudstone of the Palma Marker member that range compositionally from  $\text{MgCaSi}_2\text{O}_6$  to  $\text{Mg}_{0.87}\text{Fe}_{0.13}\text{CaSi}_2\text{O}_6$ . The individual grains have an irregular zonation with the outer margins containing an irregular patchy zonation of augite  $(\text{Ca}_{0.5}\text{Mg}_{0.5})(\text{Fe}_{0.19}\text{Mg}_{0.65}\text{Al}_{0.16})\text{Si}_2\text{O}_6$ , with a rim of hedenbergite. The porphyroblasts have microscopic inclusions of fluoroapatite  $\text{Ca}_5(\text{PO}_4)_3\text{F}$  and rare zircon. They are suspended in a matrix of recrystallized calcite. At the margins of the porphyroblasts and in the matrix, minor pentlandite occurs. These Mg-rich diopside porphyroblasts occur exclusively in the ~20-m-thick mudstone interval. The mudstone must have been subject to hydrothermal alteration, modifying the bulk composition of the rocks. A strong compositional control on the formation of the porphyroblasts may explain why diopside is not present elsewhere in the host rock succession.

In addition to the contact metamorphic overprint that affected the entire host rock succession of the Palma deposit and the massive sulfides, the intrusion of the Miocene dikes resulted in local contact metamorphism around these intrusions. Where the dikes crosscut intensely carbonate-altered rocks or massive sulfides, skarn-like assemblages have developed, typically within <1 m of the intrusions. At the immediate contact, the carbonate has recrystallized to massive, creamy white, semi-homogenous marble. In thin section, the carbonate minerals form a granoblastic texture of interlocking calcite grains with minor recrystallized granoblastic quartz grains and hedenbergite along the recrystallized boundaries (Fig. 1.12). Away from the intrusion, the marble grades into a creamy, light green material with relict, laminated mudstone textures (Fig. 1.12). Hedenbergite occurs within these zones of contact metamorphism, with varying proportions of Fe. Calculated mineral formula range from  $\text{Fe}_{0.65}\text{Mg}_{0.26}\text{Mn}_{0.08}\text{CaSi}_2\text{O}_6$  to  $\text{Fe}_{0.51}\text{Mg}_{0.4}\text{Mn}_{0.09}\text{CaSi}_2\text{O}_6$ . Pyrrhotite occurs occasionally in the hedenbergite-bearing assemblage as disseminations and as bands that are <4 mm wide. Where the dikes have intruded through

massive sulfides, pyrite has been converted to pyrrhotite. In some cases, the margins of the intrusions are surrounded by ~6 cm wide pyrrhotite halos that grade outward into recrystallized pyrite and sphalerite. The pyrite in these aureoles forms up to 1 cm large crystals.

## **1.7. Discussion**

### **1.7.1. Depositional environment**

The Palma deposit is hosted by carbonaceous mudstone succession that has formed by suspension sedimentation in a submarine environment. Although the host rock stratigraphy is capped by a fine-grained limestone, there is no evidence for a shallow marine depositional environment throughout the entire succession. The absence of shallow-marine sedimentary structures such as wave ripples or hummocky cross-bedding confirms that deposition occurred below storm wave base, (10–200 m water depth; Johnson and Baldwin, 1996) in a presumably relatively deep marine setting. Palma was a depocenter at, and after, the time of massive sulfide formation. The fine-grained siliciclastic material deposited by suspension sedimentation is interpreted to represent a product of erosion from a nearby landmass or islands. Thin section inspections did not reveal the presence of volcanic ash in the carbonaceous mudstone, suggesting a lack of nearby subaerial volcanic activity. However, the intrusion of mafic sills and dikes into the siliciclastic succession suggests that Palma formed in a volcanically active, extensional marginal basin (cf. Atherton et al., 1983).

### **1.7.2. Nature of the host rock succession**

The Cretaceous VMS deposits of the Western Cordillera of Peru have formed in diverse volcanological settings. The two largest deposits, Tambogrande in the Lacones region and Cerro Lindo in Cañete region, are hosted in Albian to Turonian bimodal volcanic succession and formed in close spatial and temporal association with submarine felsic volcanic centers. In contrast to these deposits, Palma is hosted in a Maastrichtian to Danian succession that primarily comprises carbonaceous mudstone intruded by mafic sills and dikes. Using the classification of Barrie and Hannington (1999), Palma is hosted by a mafic-siliciclastic host rock succession.

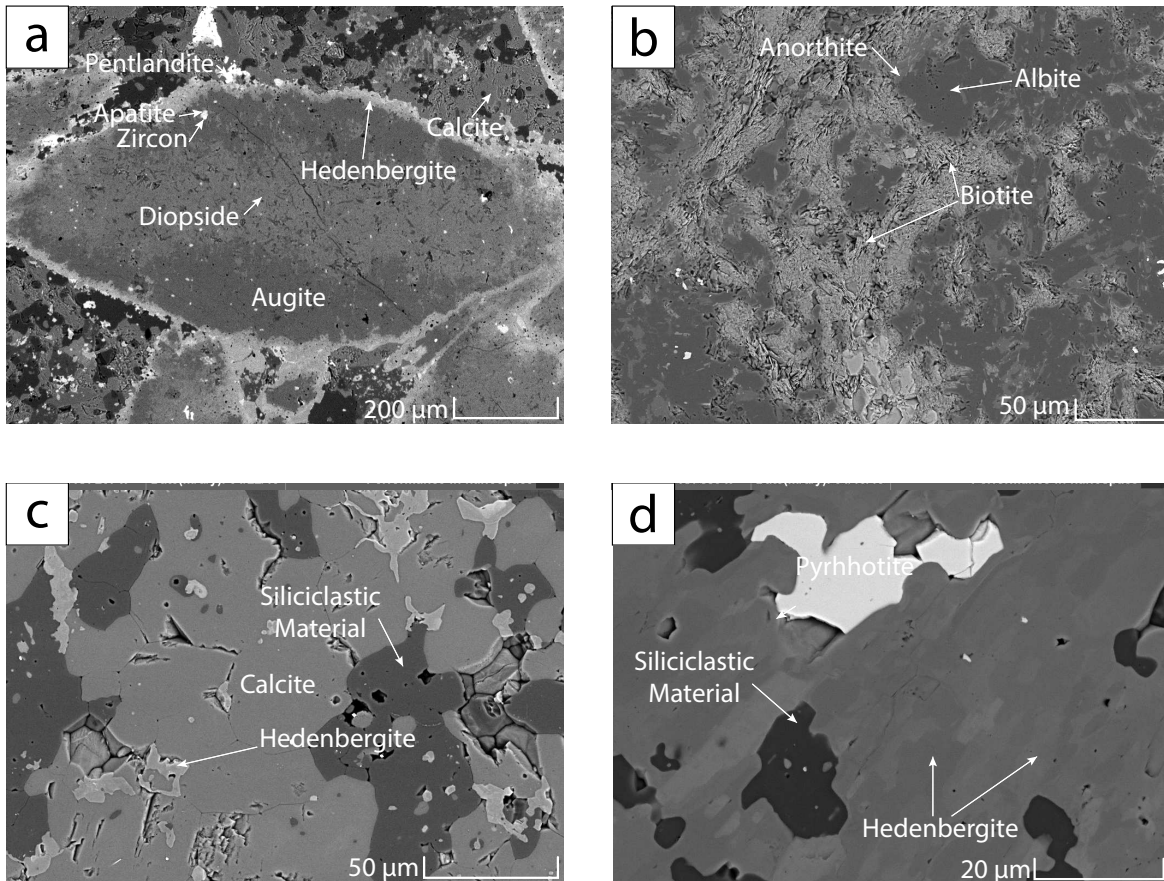


Figure 1.12. Backscattered electron images of minerals formed as a result of the metamorphic overprint. a. Diopside porphyroblast in Palma Marker member. b. Fine-grained, patchy biotite overprint in Palma-Basalt member. c. Calcite-dominant metamorphic assemblage at contact between carbonaceous mudstone and a Miocene dike. d. Hedenbergite occurring in carbonaceous mudstone at contact the contact with a Miocene dike.

Palma shares many characteristics with other deposits hosted by mafic-siliciclastic host rock successions such as the Besshi deposit on Shikoku Island, Japan (Hutchinson, 1980; Franklin et al., 1981; Slack, 1997). Shared characteristics include the conformable, stratiform, blanket-like nature of the massive sulfide lenses that are hosted by carbonaceous mudstone and subordinate graywacke. In all of these deposits, the siliciclastic host rock successions contain variable amounts of mafic dikes and sills, but generally lack felsic volcanic rocks. However, Palma exhibits a metal association that is not typically encountered in VMS deposits with mafic-siliciclastic host rock successions, Palma is primarily a Zn-Pb-Ag deposit that, as far as currently known, contains only subordinate amounts of Cu mineralization. This is in contrast to most other deposits hosted in mafic-siliciclastic successions, which tend to be Cu-rich and only have low Zn and Pb concentrations. In terms of metal association, Palma is similar to the Zn-Pb-Ag-rich Triassic Greens Creek deposit in southeastern Alaska that is also hosted by carbonaceous mudstone intruded by mafic sills and dikes (Sack, 2009; Sack et al., 2016).

The setting in which the Palma deposit formed was vent proximal. Logging of the exploration drill core conclusively showed the intrusion of many of the early mafic sills and dikes occurred into the carbonaceous mudstone when the mudstone was still wet and unconsolidated, resulting in the formation of mudstone-matrix basalt breccias along the contact between the coherent mafic units and the mudstone. This breccia is interpreted to be a peperite (Skilling, 2001). The existence of peperite along the margins of the mafic sills and dikes proves that mafic volcanism was essentially contemporaneous with the background sedimentation at Palma.

The observation that the carbonaceous mudstone of the Palma Basalt member was wet and unconsolidated at the time of seafloor volcanism explains the distribution of the early mafic sills and dikes throughout the stratigraphy. Mafic intrusions are most abundant in the lower part of this member, but less common in the upper part of the Palma Basalt member. The lower part of the succession was presumably less water-laden and more compacted at the time of volcanism, allowing the emplacement of the mafic lava as intrusions. In contrast, the water content of the mud in the upper part of the Palma Basalt member was probably much higher, preventing the wet and unconsolidated mud from supporting the intrusion of mafic lava at higher stratigraphic

levels. The wet and unconsolidated nature of the mud also explains the lack of mafic lavas that were effusively emplaced on the seafloor to form massive or pillowed flows and associated autobreccia deposits. The unconsolidated mud may simply not have been able to support the weight of a lava flow, preventing high-level emplacement of mafic lavas.

### **1.7.3. Relative timing of hydrothermal activity**

Hydrothermal activity at Palma overlapped with the seafloor volcanism and the background sedimentation. The Palma deposit is characterized by an asymmetric alteration halo. Intense alteration of mudstone occurs only in the stratigraphic footwall of the Palma Marker member suggesting that this unit formed the seafloor at the time of mineralization. The hydrothermal fluid flow was most intense prior to and during deposition of the mudstone of the Palma Marker member, but decreasing in intensity during the deposition of the ~20-m-thick unit. Only the first meters of the overlying mudstone of the Palma Pelite member have been affected by hydrothermal alteration suggesting that the hydrothermal activity essentially stopped at the end of the deposition of the Palma Marker member. Alteration patterns in the basalt units are consistent with this observation. Basalt units emplaced into the mudstone prior to deposit formation have been affected by chlorite and sericite alteration, which is now represented by biotite formed during the metamorphic overprint. Biotite-bearing mafic units only occur in the stratigraphic footwall of the Palma Marker Member, within this unit, or immediately above. Mafic units lacking biotite were emplaced after the hydrothermal event and are not altered. These unaltered mafic intrusions occur throughout the stratigraphic succession.

The textural evidence at Palma suggests that early carbonate alteration at Palma occurred at a time when the host mudstone of the upper Palma Basalt member was still unconsolidated. Carbonate-altered mudstone exhibits fluidal textures with bands of carbonate-rich material wrapping around mudstone clasts that show soft-sediment deformation textures. Although the mudstone at the top of the upper Palma Basalt member was unconsolidated during mineralization, its rheological behavior appears to have varied down stratigraphy due to the increased degree of compaction. Fluidal carbonate textures are less common down stratigraphy where mudstone reacted more brittle during the alteration, forming distinct breccias consisting of

carbonaceous mudstone clasts suspended in a carbonate matrix. These brittle textures are best explained by hydrothermal brecciation of the increasingly consolidated mudstone. The textural changes are gradational down stratigraphy, with a transition zone separating both.

The available evidence suggests that the mudstone hosting the massive sulfide lenses ranged from unconsolidated at the top of the succession to semi-consolidated towards the bottom. This gradation of porosity and permeability dictated the replacement processes and sulfide textures in the ~170 m thick Palma Basalt member assessable by drilling. Observations in petroleum basins suggest that the porosity of mudstone near the seafloor is very high, up to 70–80% and increases with compaction to about 20–40% at a burial depth of 1000 m (Bjørlykke, 2015).

#### **1.7.4. Mechanisms of sulfide precipitation**

A subseafloor replacement origin of the massive sulfides at Palma suggests the existence of a steep temperature profile in the subseafloor at the time of mineralization. The sedimentary rocks of the Palma Marker member, representing the mud deposited at the time of mineralization, have only been affected by low-temperature alteration. The mudstone of the Palma Marker member exhibits banding of different colors, with some bands containing abundant diopside porphyroblasts. The presence of these porphyroblasts suggests an unusually Ca- and Mg-rich precursor composition prior to the metamorphic overprint, possibly indicating that the mudstone of the Palma Marker member may have been affected by low-temperature clay alteration. A comparable situation has been documented at the modern seafloor at Middle Valley of the northern Juan de Fuca Ridge. At this location, hemipelagic sediments in an area of active venting have been affected by moderate to intense low-temperature (mostly <150°C) hydrothermal alteration. Saponite, a Mg-rich trioctahedral smectite, represents the principal alteration mineral within the gray and blue-green mud covering the seafloor at this site (Goodfellow, 1993).

The early carbonate alteration marks an initial phase of low-temperature (<200°C) hydrothermal alteration of the Palma Basalt member. The hydrothermal fluid was able to percolate through the water-saturated, unconsolidated sediment, precipitating carbonate in inter- and intra-granular pore space and in fractures (Franklin et al. 2005). The hydrothermal fluids

appear to have been overpressured as they disrupted bedding and brecciated more compacted mudstone layers. Carbonate precipitation resulted in a reduction of the permeability, allowing a gradual increase in the thermal gradient. In addition to the change in permeability, the carbonate alteration also caused a change in the chemical reactivity of the previously unreactive siliciclastic material (Doyle and Allen, 2003).

As fluid flow through the upper part of the Palma Basalt member continued, the carbonate minerals were replaced by sulfide phases due to the progressive increases in temperature. Large (1992) showed that hydrothermal fluids are saturated in sphalerite and galena at temperatures of 175–250°C. Carbonate replacement by sulfides during prograde evolution of the hydrothermal system is demonstrated by the similarity in textures and the occurrence of sulfide replacement fronts in carbonate-rich samples

Within the lower part of the Palma Basalt member, stringer sulfides were observed in some of the deepest exploration holes. These stringers consist of pyrrhotite and chalcopyrite, indicating vein formation at even higher temperatures. Chalcopyrite precipitates at temperatures between 280 and 350 °C (Large, 1992). The chalcopyrite stringer zone identified most likely represents a high temperature upflow zone at Palma. The chalcopyrite stringers are associated with a ~40 meters wide zone of massive, patchy, high-intensity epidote veining. Epidote formation occurs at temperatures above 240 °C (Lagat, 2009).

The observations at Palma suggest that deep upflow of the hydrothermal fluids, presumably controlled by synvolcanic faults, resulted in the formation of high-temperature veins in basaltic host rocks that are Cu-rich. Due to the high permeability of the mudstone, the upwelling hydrothermal fluids cooled rapidly when they were encountering mudstone intervals between the basaltic dikes and sills. Lateral fluid flow through the permeable mudstone resulted in the formation of multiple, stacked massive sulfide lenses that are stratiform.

#### **1.7.5. Constraints on depth of seafloor replacement**

The geological relationships at Palma provide rare evidence that allows the reconstruction of the depth of replacement below the seafloor. As the original stratigraphic relationships at Palma are preserved, the depth of replacement can be approximated by measuring the distance between the paleoseafloor, which is represented by the base of the Palma Marker member, and the top of the massive sulfide lenses in core. Following subtraction of the total thickness of mafic units intersected, a distance of ~50 m is obtained. This represents a minimum depth as the mudstone in the upper part of the Palma Basalt member was not compacted at the time of mineralization.

The inferred depth of subseafloor replacement at Palma is consistent with those reported in the literature. Doyle and Allen (2003) compiled available evidence for the literature and concluded that subseafloor replacement typically occurs between meters and several hundreds of meters below the seafloor, with most examples having formed in the range of 10–200 m below the seafloor. Some of the best documented examples include the Cambrian Rosebery and Hercules deposits in Tasmania, Australia, where subseafloor replacement of highly permeable, originally pumiceous, strata occurred at up to 200 m below the seafloor (Allen, 1994).

#### **1.7.6. Comparison to other deposits hosted by mudstone-dominated successions**

In a range of VMS deposit, carbonaceous mudstone formed by suspension sedimentation represents the immediate host to massive sulfides. However, different geological relationships have been documented between the fine-grained sediments and the massive sulfides, with only few examples demonstrating that the sediments have been infiltrated and replaced by massive sulfides.

In flow-dominated volcanic successions, hemipelagic to pelagic sediment units record periods of relative volcanic quiescence. Accumulation of the fine-grained sedimentary material through suspension sedimentation requires prolonged periods of time during which effusive eruption of lavas did not occur. These periods of volcanic quiescence are required to accumulate significant amounts of massive sulfides on the seafloor. For instance, most of the mound-style massive sulfide deposits in the Archean Noranda camp of Quebec, Canada, occur at distinct stratigraphic positions within the ~2 km thick volcanic pile that are marked by the occurrence of

thin (<0.3 m) of sedimentary marker beds. Several distinct marker beds have been recognized in the camp. This includes the so-called C Contact Tuff that is host to the Amulet 11 Shaft, Amulet C, and Amulet F orebodies as well as the Lac Dufault Zinc deposit. The marker unit can be traced over a strike length of ~8 km throughout the camp (Comba, 1975; Gibson, 1990; Gibson and Galley, 2007; Bellefleur et al., 2014; Monecke et al., 2017). The stratigraphically slightly higher Main Contact Tuff of the Noranda camp hosts the D266, Amulet Lower A, East Waite, Norbec, and Vauze massive sulfide deposits (Kalogeropoulos and Scott, 1989; Gibson, 1990; Monecke et al., 2017). Both marker units are carbonaceous and contain a high proportion of volcanic ash (Monecke et al., 2017).

At the Archean Kidd Creek deposit in Ontario, Canada, a distinct carbonaceous mudstone unit that is tens of meters in thickness, occurs in the immediate hangingwall of the North orebody and the partially overlapping Central orebody. This fine-grained suspension sediment is interpreted to have been deposited prior to and during the massive sulfides, which formed by seafloor replacement in permeable volcanoclastic rocks below the accumulating mudstone. The high carbon content of the mudstone has been linked to biological activity associated with the low-temperature discharge above the North orebody (Wellmer et al., 1999). The thick mudstone unit can be traced into the footwall of the Kidd Creek South orebody, suggesting that hydrothermal activity at Kidd Creek outlived the period of suspension sedimentation resulting in the deposition of the mudstone unit.

The massive sulfides at the Triassic Greens Creek deposit in Alaska overly a footwall succession composed of mafic volcanic rocks and subordinate amounts of siliciclastic rocks. The stratigraphic hangingwall is comprised of carbonaceous mudstone and minor volcanic rocks. The massive sulfides at Greens Creek have been interpreted to have formed largely by seafloor deposition. However, the mudstone immediately overlying the massive sulfides is weakly to moderately hydrothermally altered and the alteration can be traced up to 150 m into the hangingwall, demonstrating that the hydrothermal system was still operating during deposition of the mudstone (Sack, 2009).

At the Jurassic Eskay Creek deposit in British Columbia, the formation of the precious metal-rich sulfides occurred during a period of background sedimentation marking a transition from felsic to mafic volcanism (Roth et al., 1999). The immediate footwall to the stratiform orebodies at Eskay Creek consists of coherent rhyolite and rhyolite breccia. The footwall rhyolite is overlain by black, carbonaceous mudstone. The mudstone unit ranges from less than 1 m to more than 60 m in thickness. The mudstone is laminated, thinly bedded, or massive and contains abundant intercalated, tan-colored beds of fine-grained volcanoclastic material (Britton et al., 1990; Monecke et al., 2005). The main stratiform ores at Eskay Creek occur within the carbonaceous mudstone at or near the contact with the footwall rhyolite. The largest and most precious-metal rich ore zone, referred to as the 21B zone, is composed of clastic sulfide and sulfosalt beds. In the central portion of the zone, the beds are formed by pebble- to cobble-sized sulfide and sulfosalt clasts (Britton et al., 1990; Idziszek et al., 1990; Roth et al., 1999). The beds grade laterally into thinner, finer grained, clastic beds, and laminations. The clast size and bed thicknesses also decrease stratigraphically upward, progressively thinning to fine laminations and disseminated sulfide and sulfosalt minerals within the carbonaceous mudstone (Roth et al., 1999). The clastic sulfide deposits at Eskay Creek likely formed by explosive disintegration of a massive sulfide mound exposed on the seafloor. Following the hydrothermal eruptions at the source, sulfide debris was delivered into a topographic low by mass flow deposition. Deposition of individual beds of sulfide debris occurred contemporaneously with the background sedimentation, explaining the observation that the sulfide beds are intercalated with barren mudstone (Roth et al., 1999; Monecke et al., 2005). Further up stratigraphy, the carbonaceous mudstone unit at Eskay Creek hosts a high proportion of basalt sills and dikes. Massive basalt units and associated breccias units dominate in the hanging wall of the massive sulfides suggesting the onset of a period of intense mafic volcanism (Roth et al., 1999; Monecke et al., 2005).

Significant sulfide infiltration and replacement of carbonaceous mudstone appears to have occurred only in some VMS deposits hosted by mafic-siliciclastic host rock successions. Most notably, replacement ore has been reported to occur at the Triassic Windy Craggy massive sulfide deposit in northwestern British Columbia. Mineralization is hosted within fine- to very fine grained, grey, black, brown, or silver-weathering, massive to well-laminated mudstone that

forms up to 40 m thick intervals. The mudstone contains a significant tuffaceous component that consists of dark green, chlorite-rich beds and laminae. Replacement of the mudstone by sulfides occurs primarily in the feeder zone to the two large orebodies where pyrrhotite and chalcopyrite occur along selected laminae and beds of the host mudstone (Peter and Scott, 1999).

On the modern seafloor, drilling at Middle Valley on the northern Juan de Fuca Ridge unraveled the presence of a massive sulfide mineralization on the southern flank of a sediment hill. The 35-m-high sulfide mound is topped by oxidized sulfide rubble and capped by turbiditic sediment. A second mound is exposed ~300 m to the south where the discharge of 264°C hydrothermal fluid was observed. Drilling at both mounds revealed the presence of an intensely mineralized zone at 145–210 m below seafloor. Sulfides occur as veins and bedding parallel disseminated sulfides. Sulfide impregnations occur in permeable host sediments, with sulfide concentrations reaching up to 50 vol. % (Zierenberg et al., 1998).

## **1.8. Conclusions**

The Palma VMS deposit in Peru is hosted in a Cretaceous host rock succession composed of fine-grained hemipelagic sedimentary rocks intruded by basaltic dikes and sills. The deposit consists of multiple stratiform Zn-Pb-Ag rich massive sulfide lenses stacked throughout the carbonaceous mudstone host. Textural evidence suggests that the fine-grained sedimentary host rock underwent an initial phase of carbonate alteration. The carbonate-altered rocks were subsequently replaced by the massive sulfides. Based on the geological relationships, subseafloor replacement must have occurred at least ~50 m below the paleoseafloor. The stratiform massive sulfide lenses developed within the carbonate-altered mudstone stratigraphically overlying a discordant zone of Cu-rich stringer mineralization. Although only intersected in few deep drill holes so far, sulfide stringers are locally well-developed in footwall coherent mafic rocks, possibly marking a structurally controlled hydrothermal upflow zone.

The Palma deposit represents an example of a VMS deposit that has formed by subseafloor infiltration and replacement processes in a host succession containing a high proportion of fine-grained siliciclastic rocks deposited by suspension sedimentation. Sulfide replacement required

an earlier stage of carbonate alteration, forming a host that was highly reactive and susceptible to replacement. The observations at Palma have significant exploration implications as they demonstrate that VMS deposits formed through seafloor infiltration and replacement processes are not necessarily hosted in highly permeable and glassy host rocks such as pumiceous mass-flow deposits and coarse-grained volcanoclastic deposits. Seafloor replacement processes may be more common in siliclastic-dominated volcanic successions than currently recognized. In Peru, submarine successions formed during Maastrichtian to Danian extension may be favorable for this style of massive sulfide deposits.

## REFERENCES

- Allen, R.L., 1994, Synvolcanic, subseafloor replacement model for Rosebery and other massive sulfide ores. Contentious Issues in Tasmania Geology [ext. abs.]: Contentious issues in Tasmanian geology, Hobart, Australia, Abstracts, p. 89–92.
- Atherton, M.P., and Webb, S., 1989, Volcanic facies, structure, and geochemistry of the marginal basin rocks of central Peru: *Journal of South American Earth Sciences*, v. 2, p. 241–261.
- Atherton, M.P., Pitcher, W.S., and Warden, V., 1983, The Mesozoic marginal basin of central Peru: *Nature*, v. 305, p. 303–306.
- Barrie, C.T., and Hannington, M.D., 1999, Classification of volcanic-associated massive sulfide deposits based on host-rock composition: *Reviews in Economic Geology*, v. 8, p. 1–11.
- Bellefleur, G., de Kemp, E., Goutier, J., Allard, M., and Adam, E., 2014, Seismic imaging of the geologic framework and structures related to volcanogenic massive sulfide deposits in the Archean Rouyn-Noranda district, Quebec, Canada: *Economic Geology*, v. 109, p. 103–119.
- Benavides-Cáceres, V., 1999, Orogenic evolution of the Peruvian Andes: The Andean cycle: *Society of Economic Geologists Special Publication 7*, p. 61–107.
- Bjørlykke, K., 2015, Compaction of sedimentary rocks: Shales, sandstones and carbonates, in Bjørlykke, K., ed., *Petroleum geoscience: From sedimentary environments to rock physics*: Berlin, Springer, p. 351–360.
- Britton, J.M., Blackwell, J.D., and Schroeter T.G., 1990, #21 zone deposits, Eskay Creek, northwestern British Columbia: *British Columbia Ministry of Energy, Mines and Petroleum Resources, Exploration in British Columbia 1989*, p. 197–223.
- Cobbing, E.J., Pitcher, W.S., Wilson, J.J., Baldock, J.W., Taylor, W.P., McCourt, W., and Snelling, N.J., 1981, *The geology of the Western Cordillera of northern Peru*: Institute of Geological Sciences Overseas Memoir 5, 143 p.
- Comba, C.D.A., 1975, Copper-zinc zonation in tuffaceous exhalites, Millenbach mine, Noranda, Quebec: Unpublished M.Sc. thesis, Kingston, Ontario, Canada, Queen's University, 107 p.
- Dols, T., and Monecke, T., 2018, Ore petrography of the world-class Cerro Lindo volcanic-hosted massive sulfide deposit, Peru [abs.]: *Society of Economic Geologists 2018 Conference, Keystone, Colorado, 2018, Conference Proceedings*, P018.
- Doyle, M.G., and Huston, D.L., 1999, The subsea-floor replacement origin of the Ordovician Highway-Reward volcanic-associated massive sulfide deposit, Mount Windsor Subprovince, Australia: *Economic Geology*, v. 94, p. 825–844.

- Doyle, M.G., and Allen, R.L., 2003, Subsea-floor replacement in volcanic-hosted massive sulfide deposits: *Ore Geology Reviews*, v. 23, p. 183–222.
- Franklin, J.M., Lydon, J.W., and Sangster, D.F., 1981, Volcanic-associated massive sulfide deposits: *Economic Geology 75th Anniversary Volume*, p. 485–627.
- Franklin, J.M., Gibson, H.L., Jonasson, I.R., and Galley, A.G., 2005, Volcanogenic massive sulfide deposits: *Economic Geology 100th Anniversary Volume*, p. 523–560.
- Galley, A.G., Watkinson, D.H., Jonasson, I.R., and Riverin, G., 1995, The subsea-floor formation of volcanic-hosted massive sulfide: Evidence from the Ansil deposit, Rouyn-Noranda, Canada: *Economic Geology*, v. 90, p. 2006–2017.
- Gibson, H.L., 1990, The mine sequence of the central Noranda volcanic complex: Geology, alteration, massive sulphide deposits and volcanological reconstruction: Unpublished Ph.D. thesis, Ottawa, Ontario, Canada, Carleton University, 715 p.
- Gibson, H.L., and Gamble, A.P.D., 2000, A reconstruction of the volcanic environment hosting Archean seafloor and subseafloor VMS mineralization at the Potter mine, Munroe township, Ontario, Canada [ext. abs.]: *Volcanic Environments and Massive Sulfide Deposits*, Hobart, Australia, Extended Abstracts, p. 65–66.
- Gibson, H.L., and Galley, A., 2007, Volcanogenic massive sulphide deposits of the Archean, Noranda district, Québec, in Goodfellow, W.D., ed., *Mineral deposits of Canada: A synthesis of major deposit-types, district metallogeny, the evolution of geological provinces, and exploration methods*: Mineral Deposits Division, Geological Association of Canada, Special Publication no. 5, p. 533–552.
- Gibson, H.L., and Kerr, D.J., 1993, Giant volcanic-associated massive sulfide deposits: With emphasis on Archean deposits: *SEG Special Publications 2*, p. 319–348.
- Gibson, H.L., Watkinson, D.H., Watkins, J.J., Labrie, M., and Doiron, G., 1993, Volcanic reconstruction of the Corbet breccia pile, and Cu-Zn massive sulfide deposit, Noranda, Quebec: *Exploration and Mining Geology*, v. 2, p. 1–16.
- Gibson, H.L., Morton, R.L., and Hudak, G.J., 1999, Submarine volcanic processes, deposits, and environments favorable for the location of volcanic-associated massive sulfide deposits: *Reviews in Economic Geology*, v. 8, p. 13–51.
- Goodfellow, W.D., Grapes, K., Cameron, B., and Franklin, J.M., 1993, Hydrothermal alteration associated with massive sulfide deposits, Middle Valley, northern Juan de Fuca Ridge: *Canadian Mineralogist*, v. 31, p. 1025–1060.
- Hannington, M.D., Bleeker, W., and Kjarsgaard, I., 1999, Sulfide mineralogy, geochemistry, and ore genesis of the Kidd Creek deposit: Part I. North, Central, and South orebodies: *Economic Geology Monograph*, v. 10, p. 163–224.

- Hutchinson, R.W., 1980, Massive base metal sulphide deposits as guides to tectonic evolution: Geological Association of Canada Special Paper 20, p. 659–684.
- Idziszek, C., Blackwell, J., Fenlon, R., McArthur, G., and Mallo, D., 1990, The Eskay Creek discovery: Mining Magazine, March 1990, p. 172-173.
- Johnson, H.D., and Baldwin, C.T., 1996, Shallow clastic seas, in Reading, H.G., ed., Sedimentary environments: Processes, facies and stratigraphy: Oxford, Blackwell Science, p. 232–280.
- Kalogeropoulos, S.I., and Scott, S.D., 1989, Mineralogy and geochemistry of an Archean tuffaceous exhalite: The Main Contact Tuff, Millenbach mine area, Noranda, Quebec: Canadian Journal of Earth Sciences, v. 26, p. 88–105.
- Lagat, J., 2009, Hydrothermal alteration mineralogy in geothermal fields with case examples from Olkaria Domes geothermal field, Kenya [ext. abs.]: Short Course IV on Exploration for Geothermal Resources, Lake Naivasha, Neya, 2009, Extended Abstracts, 24 p.
- Large, R.R., 1992, Australian volcanic-hosted massive sulfide deposits: Features, styles, and genetic models: Economic Geology, v. 87, p. 471–510.
- León, W., de la Cruz, O., Rosell, W., and Torres, V., 2002, Mapa geologic del cuadrángulo de Lurín 25 j (1546): Instituto Geológico Minero y Metalúrgico, Perú, 1 map sheet at a 1:100,000 scale.
- Monecke, T., Gibson, H., Dubé, B., Laurin, J., Hannington, M.D., and Martin, L., 2008, Geology and volcanic setting of the Horne deposit, Rouyn-Noranda, Québec: Initial results of a new research project: Geological Survey of Canada Current Research 2008-9, 16 p.
- Monecke, T., Gale, D., Roth, T., and Hannington, M.D., 2005, The submarine volcanic succession hosting the massive sulfide and sulfosalt Eskay Creek deposit, Canada [ext. abs.] Biennial meeting of the Society for Geology Applied to Mineral Deposits, 8th, Beijing, China, 2005, Proceedings, p. 655–658.
- Monecke, T., Gibson, H.L., and Goutier, J., 2017, Volcanogenic massive sulfide deposits of the Noranda camp: Reviews in Economic Geology, v. 19, p. 169–223.
- Montelius, C., Allen, R.L., Svenson, S.Å., and Weihed, P., 2007, Facies architecture of the Palaeoproterozoic VMS-bearing Maurliden volcanic centre, Skellefte district, Sweden: GFF, v. 129, p. 177–196.
- Morton, R.L., Walker, J.S., Hudak, G.J., and Franklin, J.M., 1991, The early development of an Archean submarine caldera complex with emphasis on the Mattabi cash-flow tuff and its relationship to the Mattabi massive sulfide deposit: Economic Geology, v. 86, p. 1002–1011.

- Myers, J.S., 1974, Cretaceous stratigraphy and structure, western Andes of Peru between latitudes 10°–10°30': The American Association of Petroleum Geologists Bulletin, v. 58, p. 474–487.
- Myers, J.S., 1980, Geología de los Cuadrangulos de Huarmey y Huayllapampa: Boletín Servicio Geológica y Minero del Perú 33, 153 p.
- Noble, D.C., Ríos, A., Vidal, C.E., Spell, T.L., Zanetti, K.A., Angeles, C., Ochoa, J.L., and Cruz, S.R., 2005, Late Cretaceous basalt in the Río Mala valley, central Perú: Evidence for extensión and mafic amigmatism prior to Latest Cretaceous–Paleocene plutonism and silicic volcanism, in Helberg, J.A. ed., Volumen Especial No. 6 Alberto Giesecke Matto, Sociedad Geológica del Perú, p. 141–148.
- Peter, J.M., and Scott, S.D., 1999, Windy Craggy, Northwestern British Columbia: The world's largest Besshi-type deposit: Reviews in Economic Geology, v. 8, p. 261–295.
- Piercey, S.J., 2015, A semipermeable interface model for the genesis of seafloor replacement-type volcanogenic massive sulfide (VMS) deposits: Economic Geology, v. 110, p. 1655–1660.
- Polliand, M., and Fontboté, L., 2000, The Perubar Ba-Pb-Zn VHMS deposit, central Peru: Geological Association of Canada Special Publication, v. 2, p. 439–446.
- Polliand, M., Fontboté, L., and Spangenberg, J., 1999, Tracing back sulfur isotope reequilibration due to contact metamorphism: A case study from the Perubar VMS deposit, central Peru [ext. abs.] Fifth biennial SGA meeting and the tenth quadrennial IAGOD symposium, London, UK, Proceedings, p. 967–970.
- Romero, D., 2007, La cuenca Cretácico Superior-Paleoceno del Perú Central: Un metalotecto para la exploración de SMV, ejemplo mina Maria Teresa: Unpublished M.Sc. thesis, Cusco, Peru, Universidad Nacional San Antonio Abad del Cusco, 100 p.
- Roth, T., Thompson, J.T.F., and Barrett, T.J., 1999, The precious metal-rich Eskay Creek deposit, northwestern British Columbia: Reviews in Economic Geology, v. 8, p. 357–373.
- Sack, P., 2005, Characterization of footwall lithologies to the Greens Creek volcanic-hosted massive sulfide (VHMS) deposit, Alaska, USA: Unpublished Ph.D. thesis, Hobart, Australia, University of Tasmania, 415 p.
- Sack, P.J., Berry, R.F., Gemmill, J.B., Meffre, S., and West, A. (2016) U–Pb zircon geochronology from the Alexander terrane, southeast Alaska: implications for the Greens Creek massive sulphide deposit: Canadian Journal of Earth Sciences, v. 53, p. 1458–1475.
- Skilling, I.P., White, J.D.L., and McPhie J., 2002, Peperite: A review of magma-sediment mingling: Journal of Volcanology and Geothermal Research, v. 114, p. 1–17.

- Slack, J.F., 1997, Descriptive and grade tonnage models for Besshi-type massive sulphide deposits: Geological Association of Canada Special Paper 40, p. 343–371.
- Steinmüller, K., Abad, N.C., and Grant, B., 2000, Volcanogenic massive sulphide deposits in Peru: Geological Association of Canada Special Publication, v. 2, p. 423–437.
- Tegart, P., Allen, G., and Carstensen, A., 2000, Regional setting, stratigraphy, alteration and mineralization of the Tambo Grande VMS district, Piura department, northern Peru: Geological Association of Canada Special Publication, v. 2, p. 375–405.
- Vidal, C.E., 1987, Kuroko-type deposits in the middle Cretaceous marginal basin of central Peru: *Economic Geology*, v. 82, p. 1409–1430.
- Vidal C.E., 1990, El enjambre de diques, San Bartolo, Lima: *Boletín de la Sociedad Geológica del Perú*, v. 81, p. 55–62
- Wellmer, F.W., Berner, U., Hufnagel, H., and Wehner, H., 1999, Carbon isotope geochemistry of Archean carbonaceous horizons in the Timmins area: *Economic Geology Monograph* 10, p. 441–456.
- Winter, L., 2008, The genesis of ‘giant’ copper-zinc-gold-silver volcanogenic massive sulphide deposits at Tambogrande, Perú: Age, tectonic setting, paleomorphology, litho-geochemistry, and radiogenic isotopes: Unpublished Ph.D. thesis, Vancouver, Canada, The University of British Columbia, 260 p.
- Winter, L.S., Tosdal, R.M., Franklin, J.M., and Tegart, P., 2004, A reconstructed Cretaceous depositional setting for giant volcanogenic massive sulfide deposits at Tambogrande, northwestern Peru: *Society of Economic Geologists Special Publication* 11, p. 319–340.
- Winter, L.S., Tosdal, R.M., Mortensen, J.K., and Franklin, J.M., 2010, Volcanic stratigraphy and geochronology of the Cretaceous Lacones basin, northwestern Peru: Position and timing of giant VMS deposits: *Economic Geology*, v. 105, p. 713–742.
- Zierenberg, R.A., Fouquet, Y., Miller, D.J., Bahr, J.M., Baker, P.A., Bjerkgård, T., Brunner, C.A., Duckworth, R.C., Gable, R., Gieskes, J., Goodfellow, W.D., Gröschel-Becker, H.M., Guérin, G., Ishibashi, J., Iturrino, G., James, R.H., Lackschewitz, K.S., Marquez, L.L., Nehlig, P., Peter, J.M., Rigsby, C.A., Schultheiss, P., Shanks, W.C., III, Simoneit, B.R.T., Summit, M., Teagle, D.A.H., Urbat, M., and Zuffa, G.G., 1998, The deep structure of a sea-floor hydrothermal deposit: *Nature*, v. 392, p. 485–488.

APPENDIX A

SAMPLE TABLE

Table A.1 Identification of samples taken in core and hand sample used for this study.

| Sample ID # | Hole ID | Lithology           | Sample                          | Depth (m)     |
|-------------|---------|---------------------|---------------------------------|---------------|
| PLM1801A    | 18101   | Palma Basalt member | Massive sulfide                 | 463.98-464.1  |
| PLM1801B    | 18101   | Palma Basalt member | Massive sulfide                 | 464.23-464.31 |
| PLM1802A    | 18101   | Palma Basalt member | Massive sulfide                 | 464.8-464.9   |
| PLM1802B    | 18101   | Palma Basalt member | Massive sulfide                 | 464.9-465.01  |
| PLM1803     | 17074   | Palma Basalt member | Massive sulfide                 | 216.6-216.74  |
| PLM18560    | 17074   | Palma Basalt member | Massive sulfide                 | 140.12-140.18 |
| PLM1804     | 17093   | Palma Basalt member | Massive sulfide                 | 169.78-169.85 |
| PLM1805     | 17093   | Palma Basalt member | Massive sulfide                 | 184.94-185    |
| PLM1806     | 17093   | Palma Basalt member | Hornfelsesd mudstone w/ sulfide | 183.71-183.77 |
| PLM1807     | 17093   | Palma Basalt member | Hornfelsesd mudstone            | 151.94-152    |
| PLM1808     | 17093   | Palma Basalt member | Marble                          | 152.37-152.42 |
| PLM1809     | 17093   | Palma Basalt member | Massive sulfide                 | 154.73-154.77 |
| PLM1810     | 17093   | Palma Basalt member | Hornfelsesd mudstone            | 155.01-155.07 |
| PLM1811     | 17093   | Palma Basalt member | Massive sulfide                 | 155.36-155.42 |
| PLM1812     | 17074   | Palma Basalt member | Massive sulfide                 | 141.43-151.5  |
| PLM1813     | 17074   | Palma Basalt member | Massive sulfide                 | 141.28-141.35 |

Table A.1 continued

|          |       |                     |                          |               |
|----------|-------|---------------------|--------------------------|---------------|
| PLM1814  | 17074 | Palma Basalt member | Massive sulfide          | 193.56-193.65 |
| PLM1815  | 17074 | Palma Basalt member | Massive sulfide          | 223.25-223.31 |
| PLM1816  | 17093 | Palma Basalt member | Massive sulfide          | 138.2-138.28  |
| PLM1817  | 17093 | Palma Basalt member | Massive sulfide          | 197.36-197.44 |
| PLM1818  | 17093 | Palma Basalt member | Late basalt              | 63.98-64.33   |
| PLM1819  | 17093 | Palma Basalt member | Late basalt              | 86-86.63      |
| PLM18221 | 17067 | Palma Basalt member | Massive sulfide          | 109.42-109.51 |
| PLM1820  | 17067 | Palma Basalt member | Massive sulfide          | 108.25-108.33 |
| PLM18750 | 18101 | Palma Basalt member | Hornfelsed mudstone      | 468.19-468.29 |
| PLM18P15 | 17067 | Palma Basalt member | Massive sulfide          | 83.29-83.39   |
| PLM18P9A | 17067 | Palma Basalt member | Massive sulfide          | 76.92-77.02   |
| PLM18P9  | 17067 | Palma Basalt member | Massive sulfide          | 77.27-77.37   |
| PLM1821  | 15057 | Palma Basalt member | Late basalt              | 263.7-264.11  |
| PLM1822  | 18101 | Palma Basalt member | Wispy calcite w/ sulfide | 392.75-392.83 |
| PLM1823  | 18101 | Palma Basalt member | Massive sulfide          | 458.65-458.73 |
| PLM1824  | 18101 | Palma Basalt member | Massive sulfide          | 459.45-459.55 |
| PLM1825  | 17093 | Palma Basalt member | Massive sulfide          | 331.2-331.23  |
| PLM18808 | 15057 | Palma Basalt member | Massive sulfide          | 470.46-470.55 |
| PLM18269 | 18107 | Palma Basalt member | Massive sulfide          | 534.21-534.31 |
| PLM18287 | 18101 | Palma Basalt member | Massive sulfide          | 453.17-453.26 |
| PLM18270 | 18107 | Palma Basalt member | Hornfelsed mudstone      | 548.23-549    |
| PLM18290 | 18101 | Palma Basalt        | Massive sulfide          | 494.38-494.44 |

Table A.1 continued

|          |             |                        |   |               |
|----------|-------------|------------------------|---|---------------|
| PLM18238 | 18101       | Palma Basalt member    | Massive sulfide                         | 538.44-538.52 |
| PLM18289 | 18101       | Palma Basalt member    | Massive sulfide                         | 553.08-553.16 |
| PLM18265 | 18107       | Palma Basalt member    | Late Basalt/hornfelsed mudstone contact | 490.66-490.72 |
| PLM18266 | 15057       | Palma Basalt member    | Late basalt                             | 502.99-503.77 |
| PLM1826  | 15057       | Palma Basalt member    | Late basalt                             | 617-617.4     |
| PLM1827  | 15057       | Palma Basalt member    | Late basalt                             | 595.4-595.9   |
| PLM1828  | 15057       | Palma Basalt member    | Early basalt                            | 575.3-575.6   |
| PLM1829  | 15057       | Palma Basalt member    | Early basalt                            | 550.95-551.25 |
| PLM1830  | 15057       | Palma Basalt member    | Early basalt                            | 583-583.3     |
| PLM1831  | 15057       | Palma Basalt member    | Early basalt                            | 457.95-458.25 |
| PLM1832  | 15057       | Palma Pelitemember     | Late basalt                             | 264.3-264.6   |
| PLM1833  | 15057       | Palma Pelite member    | Mudstone                                | 88.85-89.15   |
| PLM1834  | 15057       | Palma Marker member    | Diopside porphyroblasts                 | 312.35-312.65 |
| PLM1835  | 15057       | Palma Basalt member    | Early basalt                            | 580.77-580.97 |
| PLM1837  | Hand sample | PalmaMarker member     | Diopside porphyroblasts                 | Hand sample   |
| 1840     | Hand sample | Palma Limestone member | Limestone                               | Hand sample   |
| 1841     | 17093       | Palma Basalt member    | Wispy calcite-mud                       | 70-70.3       |